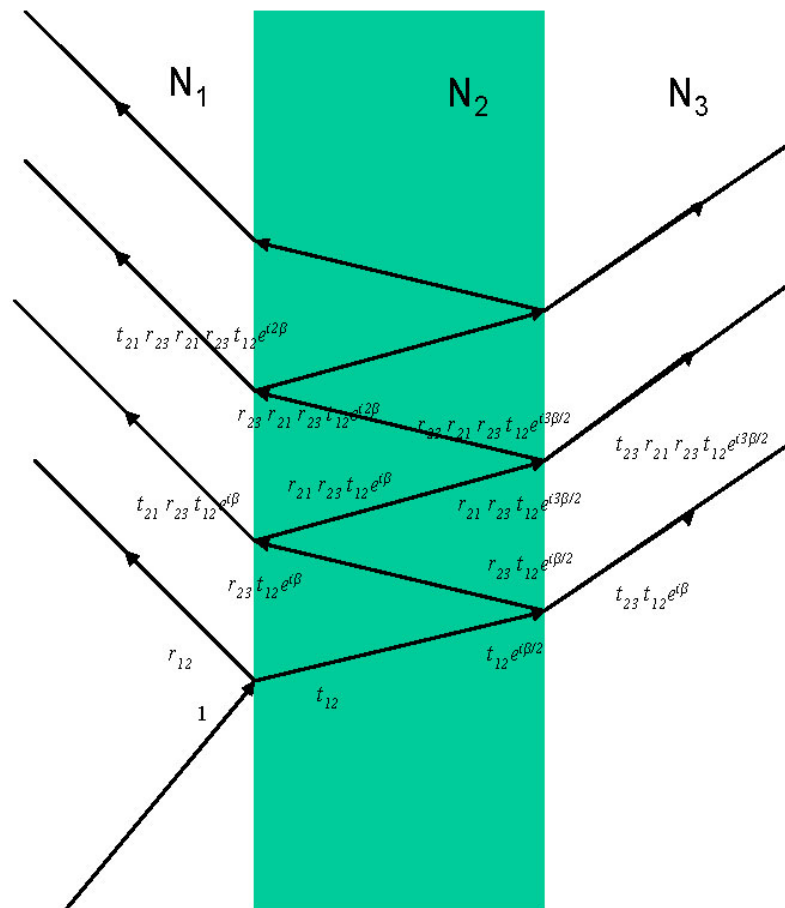




A Computational Tool for Simulating Plane Wave Reflectance from Layered Lossy Media

John O. Curtis

February 2005



A Computational Tool for Simulating Plane Wave Reflectance from Layered Lossy Media

John O. Curtis

*Environmental Laboratory
U.S. Army Engineer Research and Development Center
3909 Halls Ferry Road
Vicksburg, MS 39180-6199*

Final report

Approved for public release; distribution is unlimited

Prepared for U. S. Army Corps of Engineers
Washington, DC 20314-1000

ABSTRACT: A computational tool was developed to visualize radar reflection coefficients for a lossy, two-layered half-space soil geometry as a function of incidence angle. Allowable input parameters include radar frequency, top soil layer thickness, and the complex dielectric properties of both soil layers. The tool is a Microsoft Excel program that can operate on any Windows-based personal computer.

DISCLAIMER: The contents of this report are not to be used for advertising, publication, or promotional purposes. Citation of trade names does not constitute an official endorsement or approval of the use of such commercial products. All product names and trademarks cited are the property of their respective owners. The findings of this report are not to be construed as an official Department of the Army position unless so designated by other authorized documents.

DESTROY THIS REPORT WHEN IT IS NO LONGER NEEDED. DO NOT RETURN TO THE ORIGINATOR.

Contents

Preface	vi
1—Introduction	1
2—An Approach to Modeling Layered Lossy Media	3
Governing Equations	3
Half-space horizontal polarization	3
Half-space vertical polarization	4
The three-layer problem	4
Solution and Display Tool	5
3—Simulations of Textbook Problems	6
4—Three Studies on the Effects of Material Properties	19
Half-Space Model vs Layered Soil Model	19
A Growing Layer of Moist Soil Over Dry Soil	22
Low-Conductivity vs High-Conductivity Soils	31
5—Summary and Conclusions	39
References	41
Maxwell’s Equations	1
The Wave Equation	2
Electric Field and Magnetic Field Solutions	3
Reflection and Refraction Fields	5
Boundary Conditions	6
Amplitude Reflection and Transmission (Refraction) Coefficients	7
Horizontal polarization	7
Vertical polarization	9
Brewster’s Angle and the Critical Angle	10
Phase Shifts and Amplitude Attenuation	1
Multiple Reflections	3

SF 298

List of Figures

Figure 1.	Reflectance at an air-glass interface	7
Figure 2.	Reflectance from fresh water.....	8
Figure 3.	Reflectance from a low-loss soil	9
Figure 4.	Reflectance from sea water	10
Figure 5.	Reflectance from a nickel surface	12
Figure 6.	Reflectance from a glass-air interface	13
Figure 7.	Normal incidence reflectance from coated glass	14
Figure 8.	Normal incidence reflectance from a dielectric coating over water	15
Figure 9.	Normal incidence reflectance from a dielectric coating over water	16
Figure 10.	Oblique incidence reflectance from a dielectric coating over water	17
Figure 11.	Normal incidence reflectance from a sheet of water	18
Figure 12.	Reflectance from a half-space of moist, moderately conductive soil.....	20
Figure 13.	Reflectance from a thin, moist, moderately conductive soil layer over dry soil.....	21
Figure 14.	Layered soil reflectance vs top-layer thickness at normal incidence.....	23
Figure 15.	Layered soil reflectance vs top-layer thickness at 30 deg incidence.....	24
Figure 16.	Layered soil reflectance vs top-layer thickness at 60 deg incidence.....	25
Figure 17.	Reflectance from a dry soil half-space	26
Figure 18.	Reflectance from a 5-cm moist layer over a dry soil.....	27
Figure 19.	Reflectance from a 10-cm moist layer over a dry soil.....	28
Figure 20.	Reflectance from a 15-cm moist layer over a dry soil.....	29
Figure 21.	Reflectance from a 20-cm moist layer over a dry soil.....	30

Figure 22.	Impact of a growing moist soil layer on normal incidence reflectance and Brewster's angle.....	32
Figure 23.	Reflectance from a low-loss moist layer at normal incidence.....	33
Figure 24.	Reflectance from a low-loss moist layer at an incidence angle of 30 deg.....	34
Figure 25.	Reflectance from a low-loss moist layer at an incidence angle of 60 deg.....	35
Figure 26.	Reflectance from a high-loss moist layer at normal incidence.....	36
Figure 27.	Reflectance from a high-loss moist layer at an incidence angle of 30 deg.....	37
Figure 28.	Reflectance from a high-loss moist layer at an incidence angle of 60 deg.....	38
Figure A1.	Incident, reflected, and refracted waves at a plane interface.....	A5
Figure B1.	Paths of two rays incident on a slab of finite thickness.....	B2
Figure B2.	Reflection and refraction of a single ray incident on a slab of finite thickness.....	B3

Preface

The work reported in this document was performed as part of a U.S. Army Engineer Research and Development Center (ERDC) Intralaboratory Independent Research (ILIR) project for FY04 entitled “Microwave Inversion to Obtain Soil Moisture Profiles.” Mr. Gary Koh of the ERDC Cold Regions Research and Engineering Laboratory was the Principal Investigator for this project.

Dr. John O. Curtis, Environmental Systems Branch (ESB), Ecosystem Evaluation and Engineering Division (EE), Environmental Laboratory (EL), ERDC, Vicksburg, MS, was solely responsible for conducting the study reported herein. This investigation was conducted under the direct supervision of Dr. Rose Kress, Chief, ESB, and the general supervision of Dr. Dave Tazik, Chief, EE.

At the time of publication of this report, Dr. Edwin A. Theriot was Director, EL, and Dr. James R. Houston was Director of ERDC. Commander and Executive Director of ERDC was COL James R. Rowan, EN.

1 Introduction

A computational tool is needed to help engineers and scientists better interpret reflectance measurements from low-frequency radars that illuminate soils. Of particular interest is the use of such radars to make nondestructive measurements of near-surface soil moisture values. Commercial devices are available for measuring soil moisture values that rely on either the change in response of a time-domain reflectometer when inserted into soil (e.g., Dynamax 2004; Campbell Scientific 2004) or the change in shunt capacitance of an open-ended coaxial line operating in the frequency domain (Caldecott et al. 1985). In both cases, what is being measured is an apparent dielectric constant, which has been related to soil moisture values through a calibration. Furthermore, these technologies require probes being planted in the soil or a person carrying a probe to numerous point measurement locations within a test area.

Boom-mounted high-frequency backscatter radars have been used with some limited success to measure dielectric properties of surface materials and, in some cases, to predict soil moisture values. Ulaby's work at the University of Kansas in the early 1970s provided an optimistic outlook on such technology (Ulaby et al. 1974). A recommendation to use boom-mounted radars operating at 4-5 GHz in a horizontal polarization, horizontal receive mode, and pointing at the ground with an incidence angle of 7-17 deg was quoted in the literature as late as 1989 (Waite et al. 1984; Schmugge 1989). However, Ulaby and his colleagues were still not convinced as late as 1986 of what constituted an optimum measurement system design (Dobson and Ulaby 1986). Another high-frequency reflectometer was investigated in the 1980s with applications to ice that met with mixed success (Arcone and Larson 1988).

Lower frequency radars are faced with the problem of too much penetration of soil layers under certain conditions that results in reflectance values that oscillate as a function of soil layer thickness. One source identified a technique for using low-frequency radars to determine layer thicknesses and possibly layer dielectric properties (Lundien 1972). Because there is strong evidence that dielectric properties and soil moisture levels are correlated (Topp et al. 1980; Curtis 2001), one could theoretically measure dielectric properties and obtain soil moisture values.

The objective of this project was to develop a computational tool that would allow one to easily visualize radar reflection coefficients for a two-layered soil as a function of incidence angle. Among the desired input parameters were radar

frequency, top-layer thickness, and the complex dielectric properties of both soil layers. Such a tool could be used to conduct parametric studies that show the effect of top-layer thickness and soil properties on radar reflectance values and Brewster angles.

Although previous research has pointed out some of the shortcomings of both low- and high-frequency radars to accurately measure soil moisture values, it is felt that there is still room for exploring the phenomenology of the radar waves interacting with the soil layers. The hope is that a type of measurement may be discovered that will uniquely relate reflectance to soil dielectric properties and, thence, to soil moisture values. The computational tool described in this report is one means of achieving that goal.

2 An Approach to Modeling Layered Lossy Media

Governing Equations

Textbooks are replete with mathematical models for electromagnetic wave amplitude reflection and transmission coefficients (Stratton 1941; Jackson 1975). They account for complex dielectric properties (although they usually are applied to problems with real dielectric permittivities) and both horizontally and vertically polarized electric fields. They also cover oblique angles of incidence. However, they are usually limited to half-space geometries. In other words, there is no allowance made for multiple layers in the nontransparent material. If a solution is offered for two layers, it is normally done for the special condition of normal incidence.

Half-space horizontal polarization

Appendix A contains the derivation of the half-space amplitude reflection coefficient and transmission coefficient relationships. For a plane electric wave whose propagation vector is perpendicular to the plane of incidence (see Figure A1), traveling from material i to material j and striking the interface with an incident angle of θ , the reflection coefficient (the ratio of reflected amplitude to incident amplitude) is:

$$r_{ij} = \frac{\cos \theta - \frac{\mu_i}{\mu_j} \sqrt{\frac{\mu_j \hat{\epsilon}_j}{\mu_i \hat{\epsilon}_i} - \sin^2 \theta}}{\cos \theta + \frac{\mu_i}{\mu_j} \sqrt{\frac{\mu_j \hat{\epsilon}_j}{\mu_i \hat{\epsilon}_i} - \sin^2 \theta}} \quad (1)$$

where

$$\hat{\epsilon}_j = \frac{\epsilon_j}{\epsilon_0} + i \frac{\sigma_j}{\epsilon_0 \omega} = \epsilon'_j + i \epsilon''_j \quad (2)$$

is what most authors agree is called the complex relative dielectric constant of material j . $\hat{\epsilon}_j$ is often called the dielectric permittivity, σ_j is the electrical conductivity of the material (mho/m), ω is the radial frequency of the wave, and ϵ_0 is the permittivity of free space (8.85×10^{-12} farads/m). μ_j is the magnetic permeability of the material.

Half-space vertical polarization

When the incident electric wave propagation vector lies within the plane of incidence, a different coefficient can be calculated:

$$r_{ij} = \frac{\cos \theta - \frac{\hat{\epsilon}_i}{\hat{\epsilon}_j} \sqrt{\frac{\mu_j \hat{\epsilon}_j}{\mu_i \hat{\epsilon}_i} - \sin^2 \theta}}{\cos \theta + \frac{\hat{\epsilon}_i}{\hat{\epsilon}_j} \sqrt{\frac{\mu_j \hat{\epsilon}_j}{\mu_i \hat{\epsilon}_i} - \sin^2 \theta}} \quad (3)$$

At normal incidence, with the wave propagating from air onto some nonmagnetic material, both coefficients are identical and reduce to the familiar form:

$$r = \frac{1 - \sqrt{\hat{\epsilon}}}{1 + \sqrt{\hat{\epsilon}}} \quad (4)$$

The vertical polarization equation produces a negative sign, which is nothing more than an artifact of how the electric field vectors were assumed to be pointing in the derivation.

The three-layer problem

One text presents a solution for electric waves obliquely incident upon a two-layer medium (Reitz et al. 1979), which has been condensed in Appendix B. For a plane wave traveling from material 1 (in this case, air) through a finite thickness layer of material 2 and then into a semi-infinite material 3, the net amplitude reflection coefficient from the first interface is:

$$r = \frac{r_{12} + r_{23} e^{i\beta}}{1 + r_{12} r_{23} e^{i\beta}} \quad (5)$$

where r_{12} and r_{23} are the half-space reflection coefficients at the first and second interface, respectively, and come from Equations 2 and 3 for each polarization condition. β is a term calculated from Equations B1 through B3 that accounts for wave attenuation through material 2 as well as a shift in phase and is a function of incidence angle, layer 2 thickness, and the complex dielectric properties of the second layer.

Obviously, this net amplitude reflection coefficient can be a complex number, indicative of phase shifts and attenuation within the top layer of material. All of the charts that will be shown in this report will be plots of the reflectance of the waves, the average energy flux per unit area. Reflectance will then be calculated from Equation 5 by the formula:

$$R = rr^* \quad (6)$$

Solution and Display Tool

An Excel file was created, a copy of which can be obtained from the author, that utilizes these equations and other relevant equations from Appendixes A and B to calculate the magnitude and phase of the various reflection and transmission coefficients as well as the intensity of the reflected energy (the magnitude squared). Once loaded into a Windows-based computer, the following procedure can be used to generate results for specific test conditions:

1. Open the file and create a second window on the display screen. In one window of the display, choose the “calculations” tab. In the other window, choose a tab for the type of chart that is desired. For example, if what is required is a visual display of the power reflectance vs angle of incidence, then choose the tab entitled “power reflection (3 layers).”
2. On the upper left corner of the “calculations” sheet, input all of the relevant operating conditions and layer properties. For example, the real and imaginary parts of the complex dielectric constant for material 2 should be entered into cells B7 and C7, respectively. Properties for material 3 are entered into row 9. The thickness of material 2 is entered into cell C14, in units of centimeters. Wave frequency is entered into cell C13. Entered data that effects a change in power reflection will immediately be seen on the other side of the split display.
3. A macro was written to calculate and display power reflectance for any incidence angle as a function of material 2 layer thickness. This chart is found at the tab entitled “power refl vs layer thickness.” With the “calculations” sheet active, simply execute the macro and view the result on the chart displayed in the other window. The macro has been written to calculate reflectances for layer thickness up to one and a half times the wavelength of the electric field in material 2. If some other incidence angle is desired, then simply edit the first line of the macro to set the incidence angle value and run the macro again.

3 Simulations of Textbook Problems

To build confidence in the computational tool, a number of textbook problems were solved, and charts of the results are presented in this chapter. Many of the published solutions were for half-space problems, not multilayered geometries. All that was done in those cases is that both layers of nontransparent material were given the same properties. Furthermore, when another author presented a multilayer problem, it most often was done for the special case of normal incidence and, therefore, did not fully exercise the computational tool. Nevertheless, those problems present the only opportunity to validate the solution technique reported herein.

The first simulation performed using this computational tool is that of reflectance at an air-glass interface. Results are shown in Figure 1, which perfectly match those found in numerous electromagnetics and optics texts (i.e., Reitz et al. 1979). Glass is taken to be a lossless material with an index of refraction equal to 1.5. Horizontal polarization refers to the situation in which the incident electric field vector is perpendicular to the plane of incidence (for the derivations in Appendix A, the plane of incidence is the plane of this page). For vertical polarization, the incident electric field lies within the plane of incidence. The Brewster angle (Equation A50) is 56.3 deg.

Reflectance charts for two relatively low-loss natural materials were found in the literature. One, shown in Figure 2, is for fresh water, while the other, shown in Figure 3, is for soil (Stratton 1941). At 100 MHz, the imaginary part of the complex dielectric constant for fresh water equates to 22.2 mS/m of effective conductivity. On the other hand, the conductivity for the soil simulation is 1.0 mS/m.

Figure 4 represents a simulation of sea water (reported in Long 1983) at a frequency of 300 MHz. The effective conductivity of the sea water was taken to be 4.3 S/m.

Another interesting simulation taken from a textbook is that for reflectance at an air-metal interface (Reitz et al. 1979). Although the equations derived in the Appendixes are for dielectric media, this computational tool was still able to accurately reproduce the published results. What is surprising is that the required

Three-Layer Model

$$\epsilonpsilon_1 = (1 , 0)$$

$$\mu_1 = (1 , 0)$$

$$\epsilonpsilon_2 = (2.25 , 0)$$

$$\mu_2 = (1 , 0)$$

$$\epsilonpsilon_3 = (2.25 , 0)$$

$$\mu_3 = (1 , 0)$$

$$\text{frequency (Hz)} = 6.00\text{E}+14$$

$$\text{2nd layer thickness (cm)} = 100.00$$

$$\text{2nd layer wavelength (cm)} = 3.33\text{E}-05$$

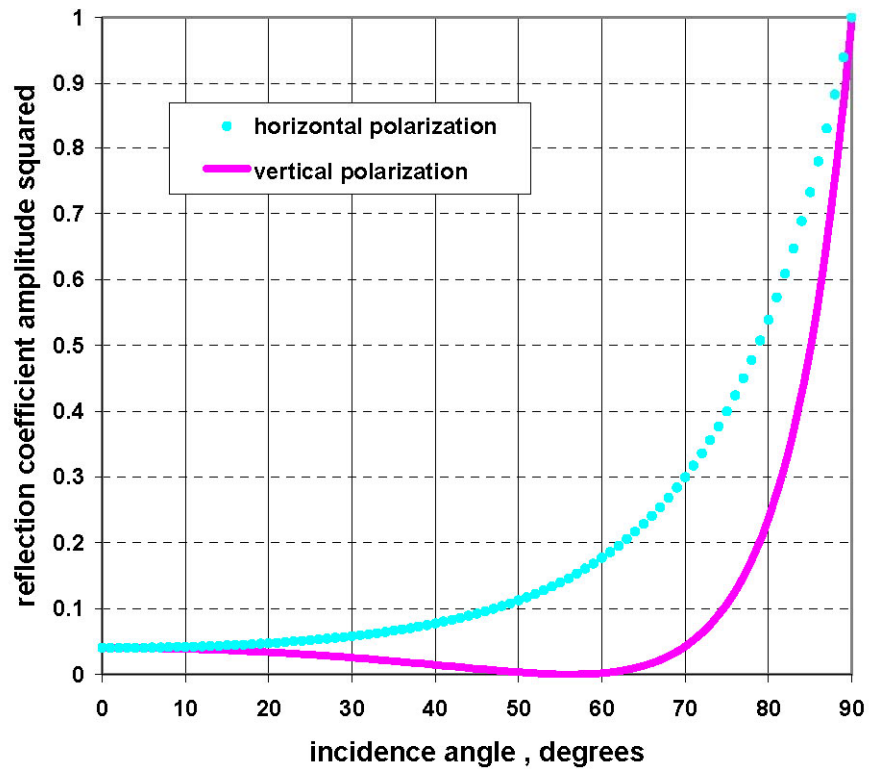


Figure 1. Reflectance at an air-glass interface

Three-Layer Model

$$\epsilon_{11} = (1 , 0)$$

$$\mu_1 = (1 , 0)$$

$$\epsilon_{21} = (81 , 4)$$

$$\mu_2 = (1 , 0)$$

$$\epsilon_{31} = (81 , 4)$$

$$\mu_3 = (1 , 0)$$

$$\text{frequency (Hz)} = 1.00\text{E}+08$$

$$\text{2nd layer thickness (cm)} = 100.00$$

$$\text{2nd layer wavelength (cm)} = 3.33\text{E}+01$$

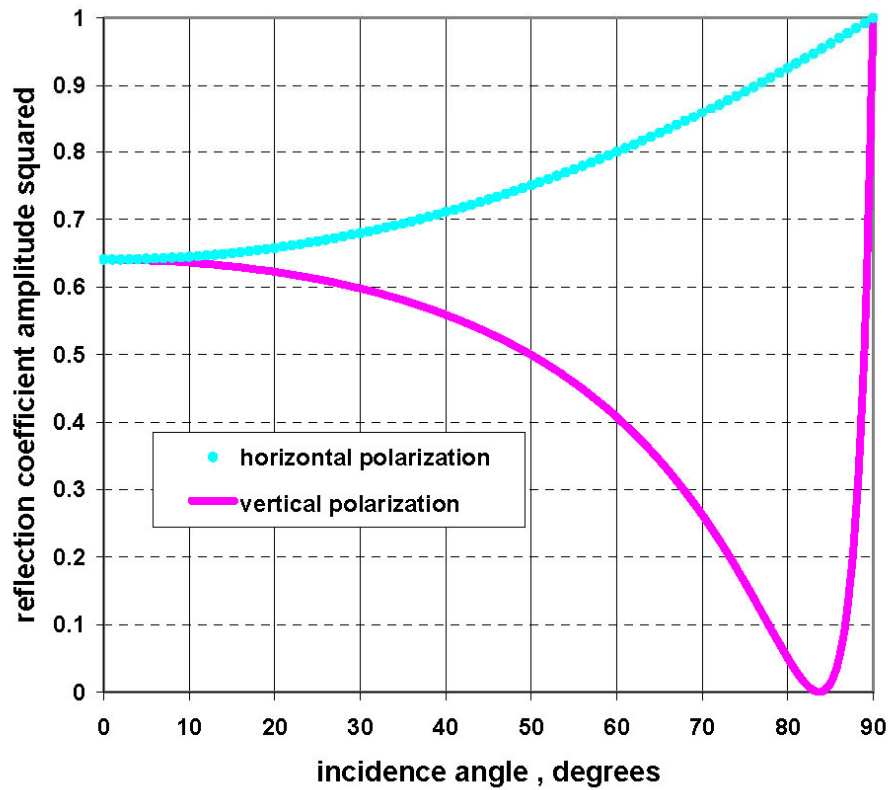


Figure 2. Reflectance from fresh water

Three-Layer Model

$$\epsilonpsilon_1 = (1 , 0)$$

$$\mu_1 = (1 , 0)$$

$$\epsilonpsilon_2 = (6 , 0.18)$$

$$\mu_2 = (1 , 0)$$

$$\epsilonpsilon_3 = (6 , 0.18)$$

$$\mu_3 = (1 , 0)$$

$$\text{frequency (Hz)} = 1.00\text{E}+08$$

$$\text{2nd layer thickness (cm)} = 100.00$$

$$\text{2nd layer wavelength (cm)} = 1.225\text{E}+02$$

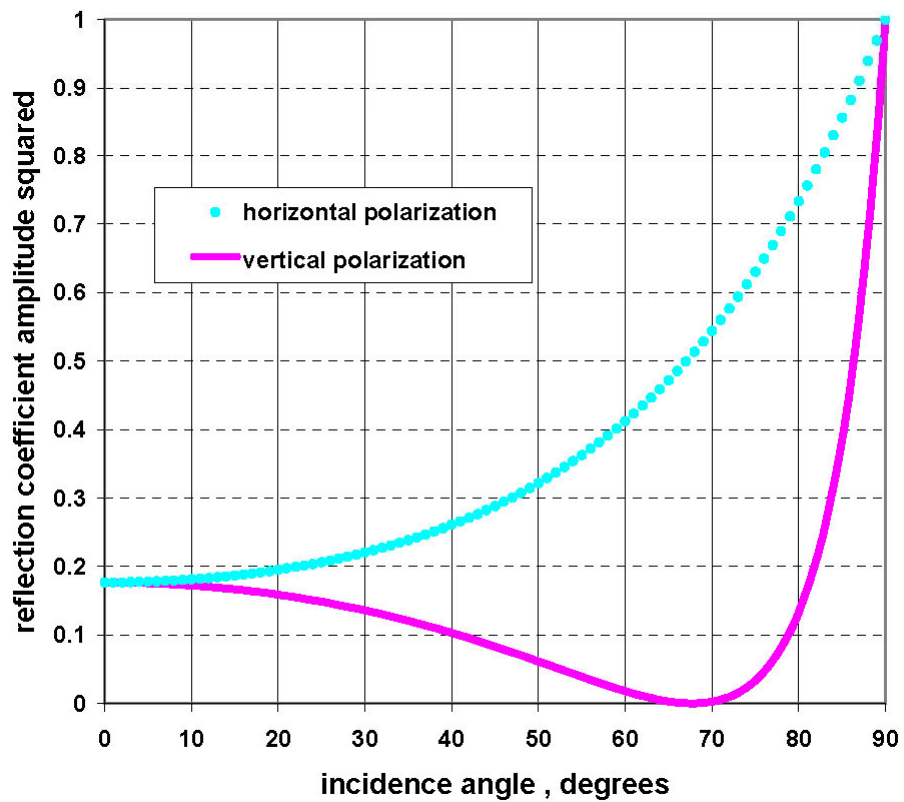


Figure 3. Reflectance from a low-loss soil

Three-Layer Model

$$\epsilonpsilon_1 = (1 , 0)$$

$$\mu_1 = (1 , 0)$$

$$\epsilonpsilon_2 = (80 , 258)$$

$$\mu_2 = (1 , 0)$$

$$\epsilonpsilon_3 = (80 , 258)$$

$$\mu_3 = (1 , 0)$$

$$\text{frequency (Hz)} = 3.00\text{E}+08$$

$$\text{2nd layer thickness (cm)} = 100.00$$

$$\text{2nd layer wavelength (cm)} = 7.56\text{E}+00$$

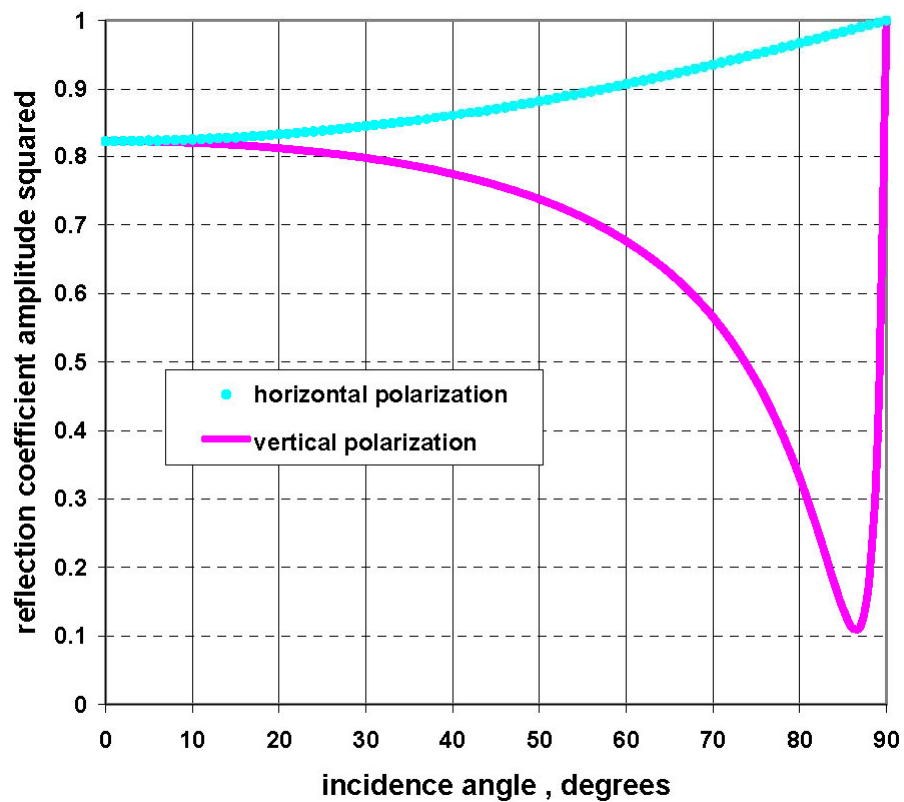


Figure 4. Reflectance from sea water

complex dielectric constant values appear to be meaningless. What is meant by this is the following. For the case of nonmagnetic materials, one can write that the complex index of refraction is related to the complex dielectric constant (combining the notations of Equations A11 and A40) by

$$N = n + ik = \sqrt{\varepsilon' + i\varepsilon''}$$

which then results in:

$$\varepsilon' = n^2 - k^2 \quad \text{and} \quad \varepsilon'' = 2nk$$

In Figure 5, the complex index of refraction for nickel was taken to be 2+i3. That value results in a complex dielectric constant of -5+i12. One is not accustomed to seeing negative values of dielectric permittivity when working with soils and other dielectrics. However, negative values are possible for metallic conductors (Klein and Furtak 1986).

While this computational tool is intended to be used for electromagnetic waves traveling from air to an air-soil interface, another check of the efficacy of the models is a simulation of the internal reflection problem; i.e., fiber optics. In this case, the conditions are that the wave is traveling from within glass to a glass-air interface. Results of the simulation are shown in Figure 6 and are exact up to the critical angle of 42 deg (Reitz et al. 1979). Beyond this angle, there is no energy entering what is called the “top layer” of material (air), and the computational tool attempts to divide by zero and fails. Results from a two-layer simulation are buried within the computational tool and can be viewed at the tab labeled “power reflection (2 layers).” Those results exactly match the published results at all angles.

A few textbook problems involving layered media are available as test cases for this computational tool. One is the problem of glass coated with a dielectric (Reitz et al. 1979), the results of which are shown in Figure 7. This is actually the classical quarter wavelength problem for reducing reflectance from optical lenses. Unfortunately, the textbook authors decided to chart the reflectance against coating thickness normalized to the free space wavelength, so that the minimum does not show up at a quarter of a wavelength within the coating.

However, another author did show results for the quarter wavelength problem plotted on a scale where the destructive interference minima are revealed at a quarter of the coating wavelength (Stratton 1941). The application, whose simulation results are shown in Figure 8, is that of a dielectric sheet over water. Perhaps the goal was to fabricate a fish tank with the least reflectance for better viewing. As the results show, minima do occur at a quarter wavelength and at multiples of half wavelength, thereafter. What is most interesting, however, is that the simulation shows zero reflectance for normal incidence when the coating dielectric constant is properly chosen. As displayed on Figure 9, zero reflectance occurs when the coating dielectric constant is the geometric mean of the constant for air and the constant for water. Figure 10 demonstrates that the

Three-Layer Model

$$\epsilonpsilon_1 = (1 , 0)$$

$$\mu_1 = (1 , 0)$$

$$\epsilonpsilon_2 = (-5 , 12)$$

$$\mu_2 = (1 , 0)$$

$$\epsilonpsilon_3 = (-5 , 12)$$

$$\mu_3 = (1 , 0)$$

$$\text{frequency (Hz)} = 6.00\text{E}+14$$

$$\text{2nd layer thickness (cm)} = 100.00$$

$$\text{2nd layer wavelength (cm)} = \text{\#NUM!}$$

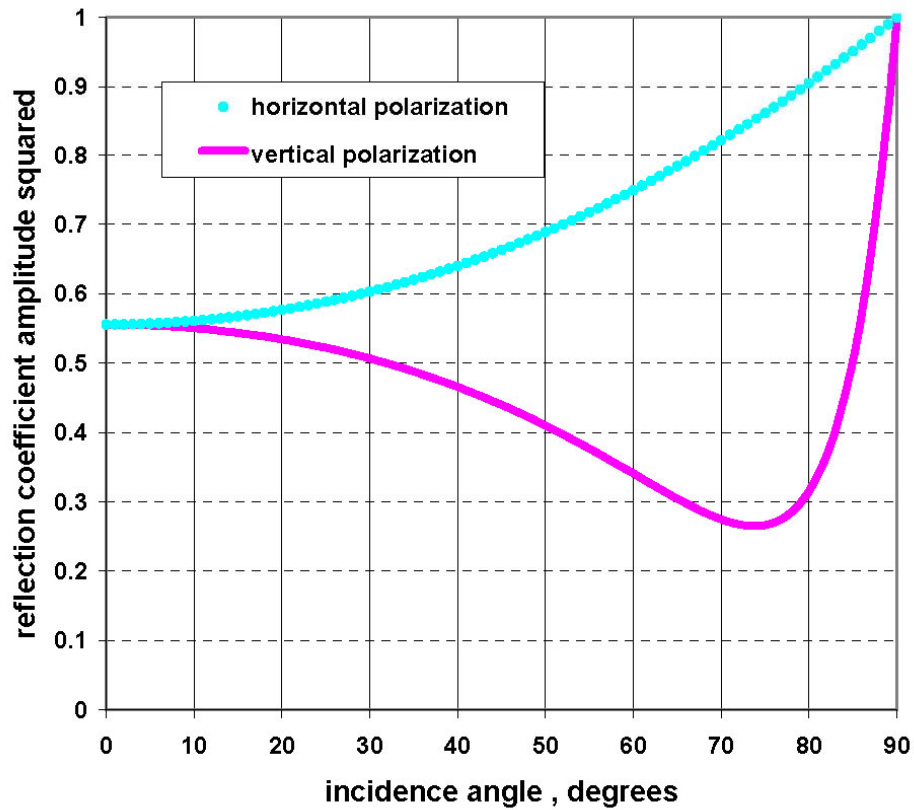


Figure 5. Reflectance from a nickel surface

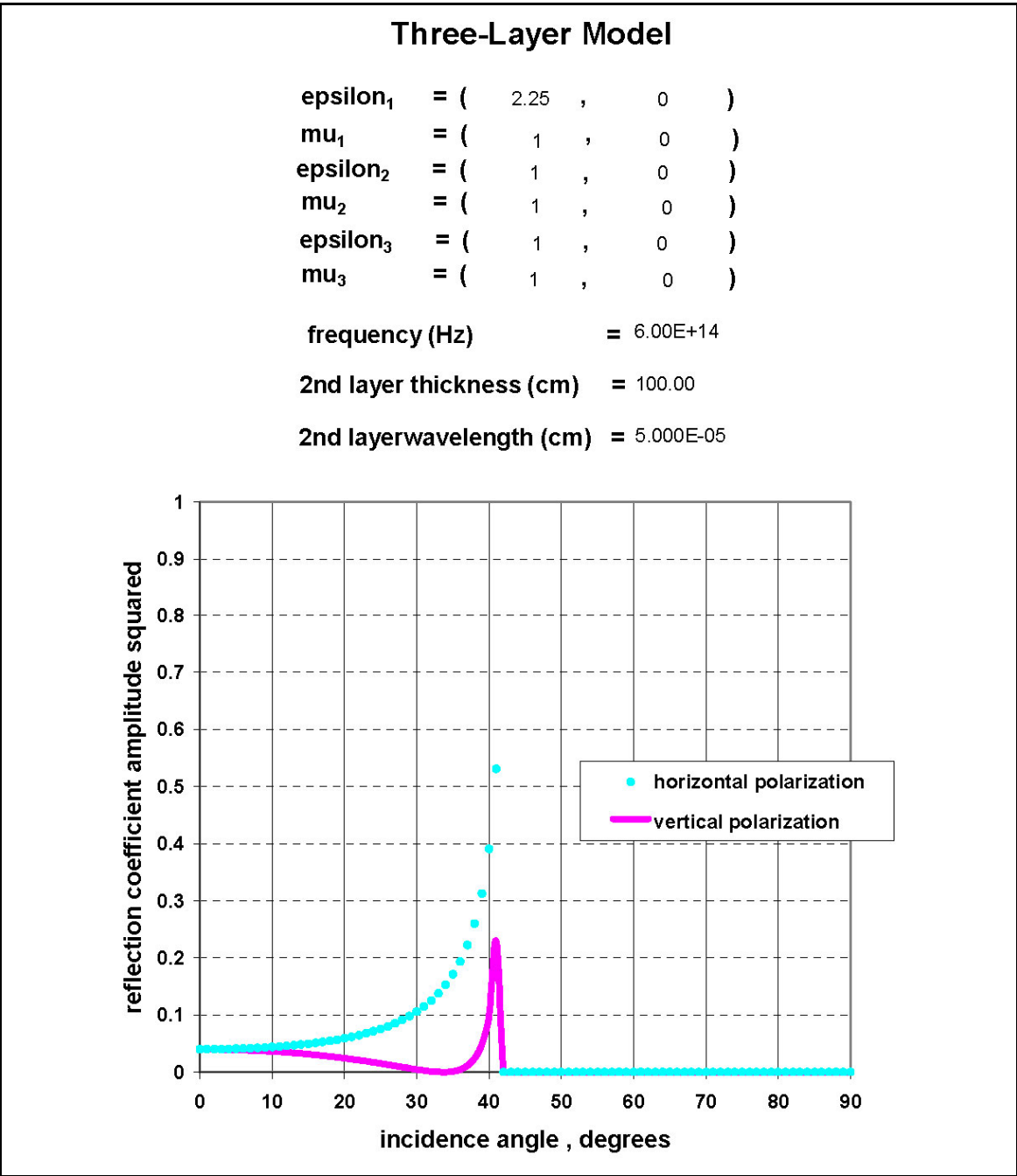


Figure 6. Reflectance from a glass-air interface (total internal reflection)

Specular Reflectance from Layered Materials

incidence angle (deg) = 0
frequency (Hz) = 6.00E+14
top layer wavelength (cm) = 3.536E-05
top layer dielectric constant = (2 , 0)
bottom layer dielectric constant = (81 , 0)

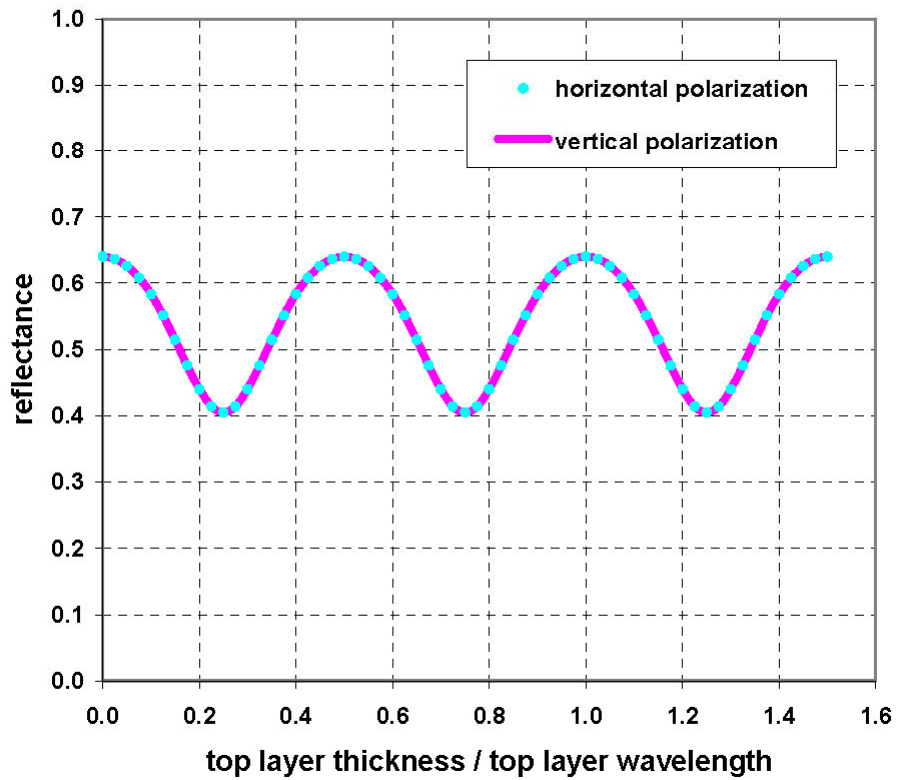


Figure 8. Normal incidence reflectance from a dielectric coating over water ($\epsilon = 2$)

Specular Reflectance from Layered Materials

incidence angle (deg) = 0
frequency (Hz) = $6.00\text{E}+14$
top layer wavelength (cm) = $1.67\text{E}-05$
top layer dielectric constant = (9 , 0)
bottom layer dielectric constant = (81 , 0)

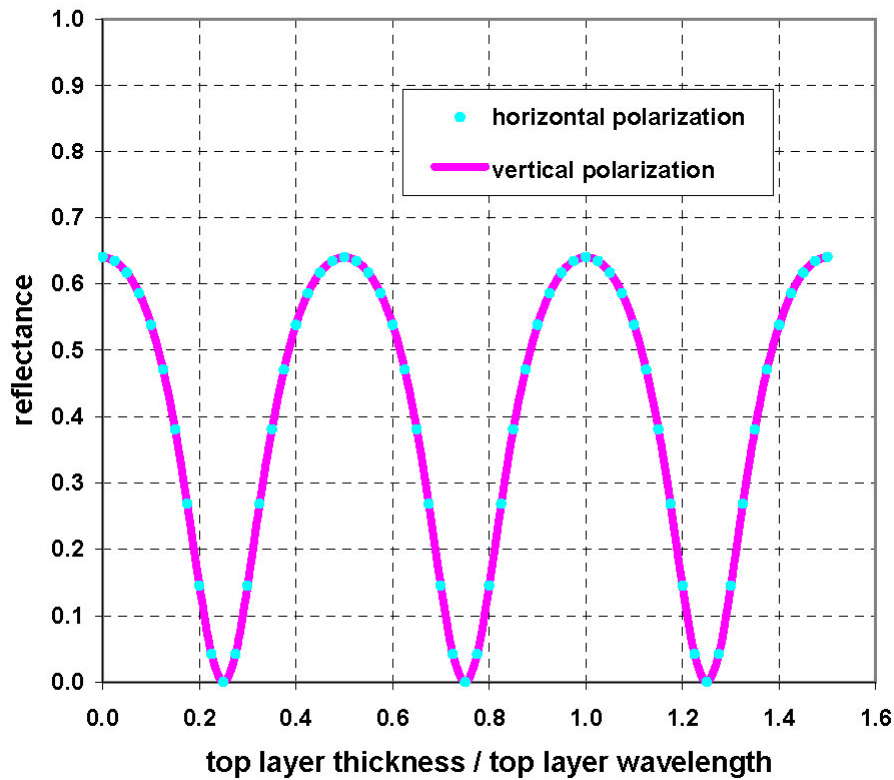


Figure 9. Normal incidence reflectance from a dielectric coating over water ($\epsilon = 9$)

Specular Reflectance from Layered Materials

incidence angle (deg) = 60
frequency (Hz) = 6.00E+14
top layer wavelength (cm) = 1.67E-05
top layer dielectric constant = (9 , 0)
bottom layer dielectric constant = (81 , 0)

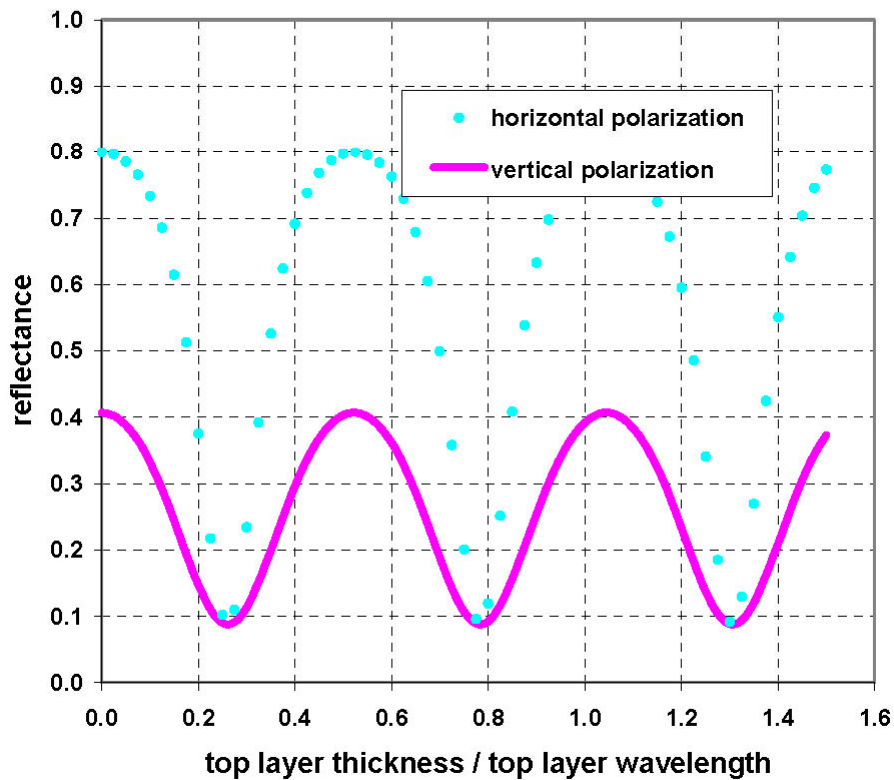


Figure 10. Oblique incidence reflectance from a dielectric coating over water ($\epsilon = 9$)

quarter wavelength effect is still pronounced at an oblique angle of incidence but that the reflectance does not go to zero at a quarter wavelength.

One final example is that of a sheet of water with air on either side (Stratton 1941). Figure 11 shows the results of this simulation using the computational tool. It demonstrates two principles. One is that reflectance minima will occur at resonant conditions set up at every half wavelength of thickness. The second principle is that since the properties of the water include a loss factor, the peak reflectance of the sheet decreases with increasing thickness because of attenuation of the wave energy.

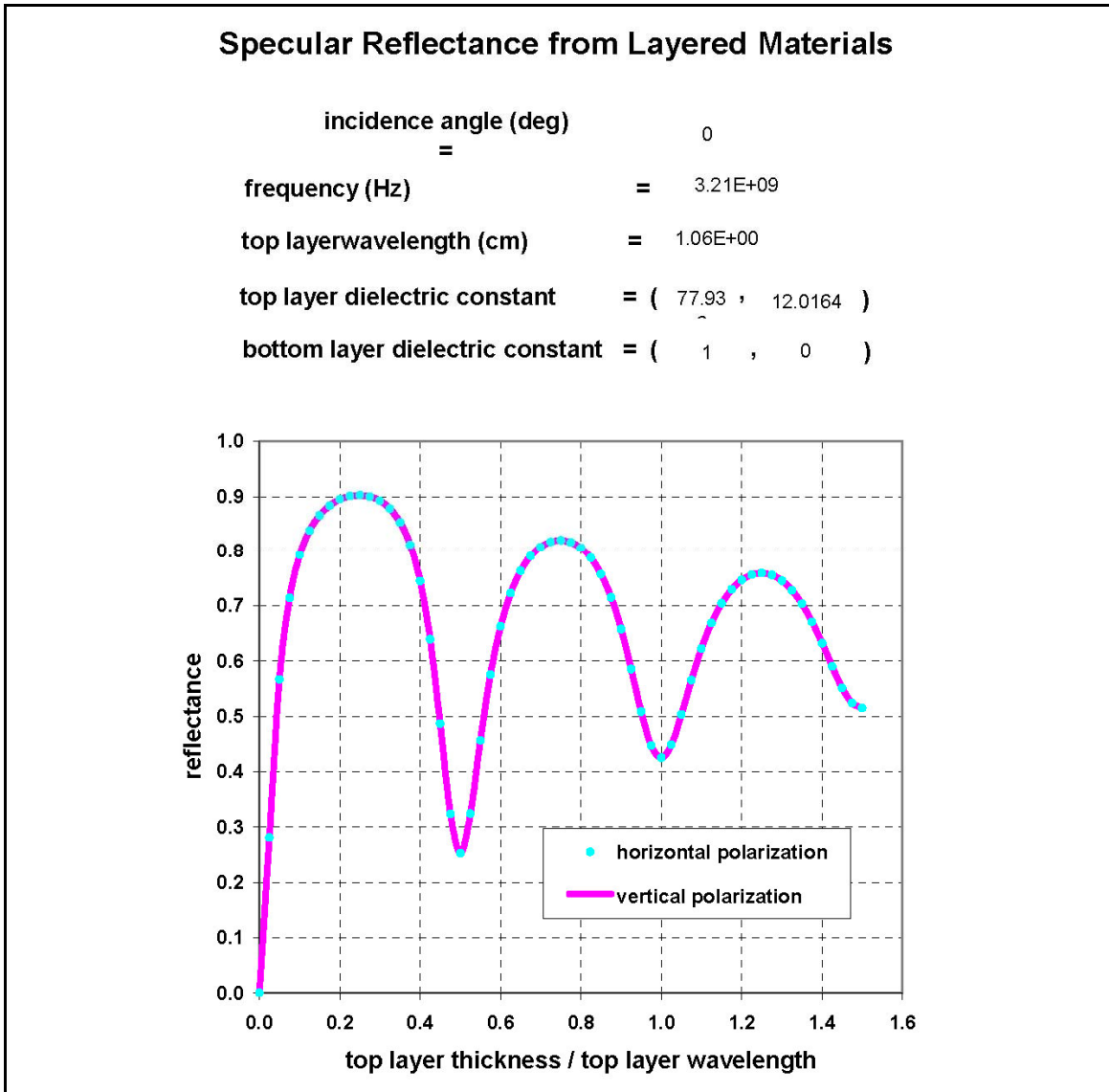


Figure 11. Normal incidence reflectance from a sheet of water

4 Three Studies on the Effects of Material Properties

Having established the worthiness of this computational tool through simulations of classical problems reported in the previous chapter, it is now time to demonstrate the effects of material properties on problems for which this tool was created; namely, layered soils. The following pages contain simulations that attempt to explore three different concerns:

1. Are half-space models “good enough” for realistic terrain?
2. What is the effect of a growing layer of moist soil?
3. How is the response of a high-conductivity soil different from that of a low-conductivity soil?

Dielectric properties for these soils were taken from data collected by the author over a period of many years. They are meant only to be typical values. Soil dielectric properties are strongly related to soil moisture and, to a lesser degree, soil temperature and bulk density (Curtis 2001). Attenuation in the soil, represented by electrical conductivity values, is clearly a function of soil chemistry (Curtis 2004) and is virtually unpredictable. Unfortunately, if one wants an accurate picture of the soil electrical properties at any given site, those soils need to be sampled and tested in a laboratory.

Half-Space Model vs Layered Soil Model

The computational tool was used to simulate a layer of moist soil having moderate conductivity on top of a relatively dry soil. The dry soil was assigned a complex dielectric constant of $3 + i0.2$, which, at a frequency of 100 MHz, translates to an effective conductivity of 1.1 mS/m. The moist soil’s dielectric constant was chosen to be $10 + i2$, which results in a conductivity of 11.1 mS/m.

One question that begs for an answer is “Does soil layer thickness make a difference at a typical ground-penetrating radar frequency?” Figure 12 is a simulation of a half-space of moist soil, while Figure 13 shows results for a 5-cm-thick layer of moist soil over dry soil. Clearly, reflectance values are

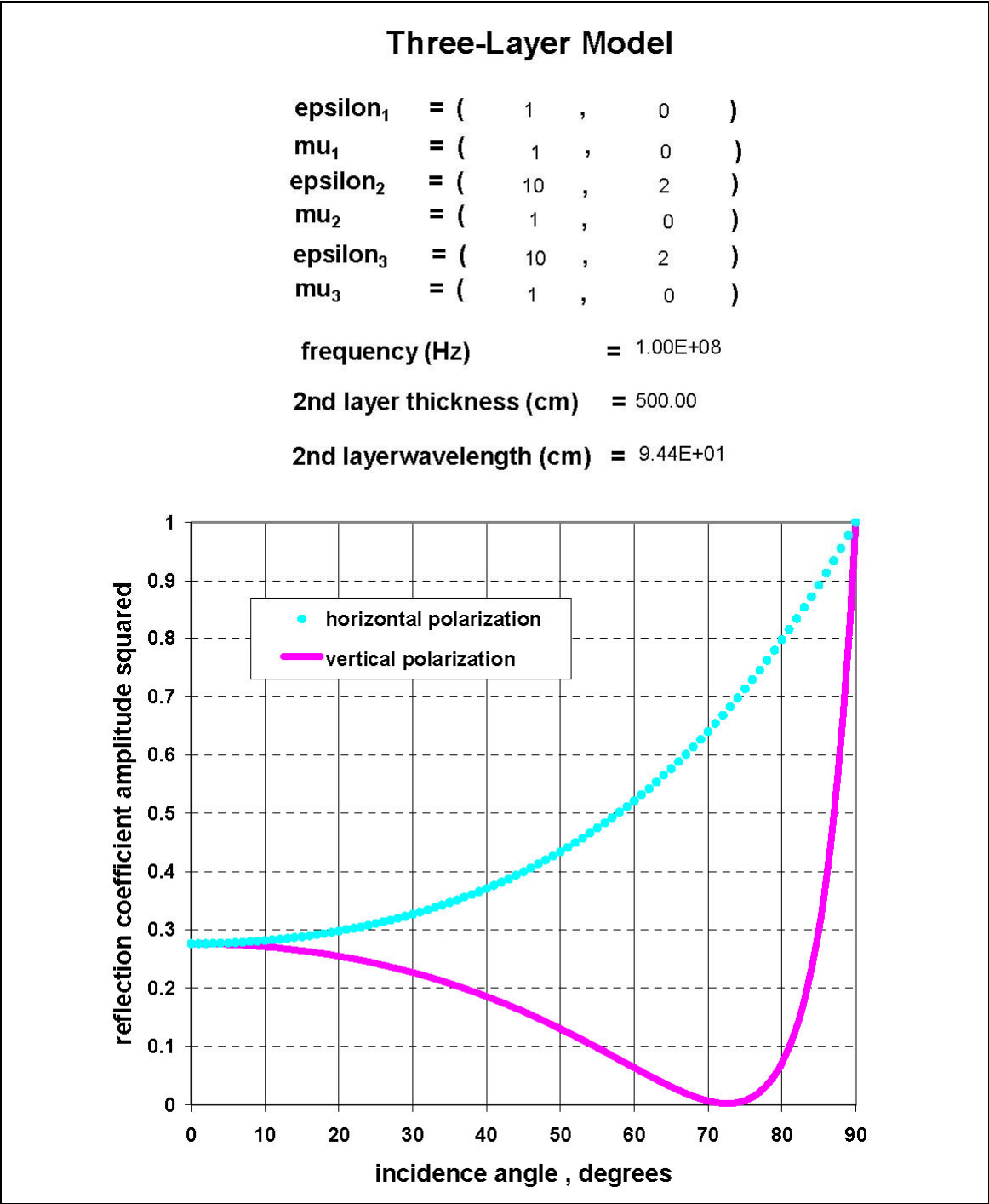


Figure 12. Reflectance from a half-space of moist, moderately conductive soil

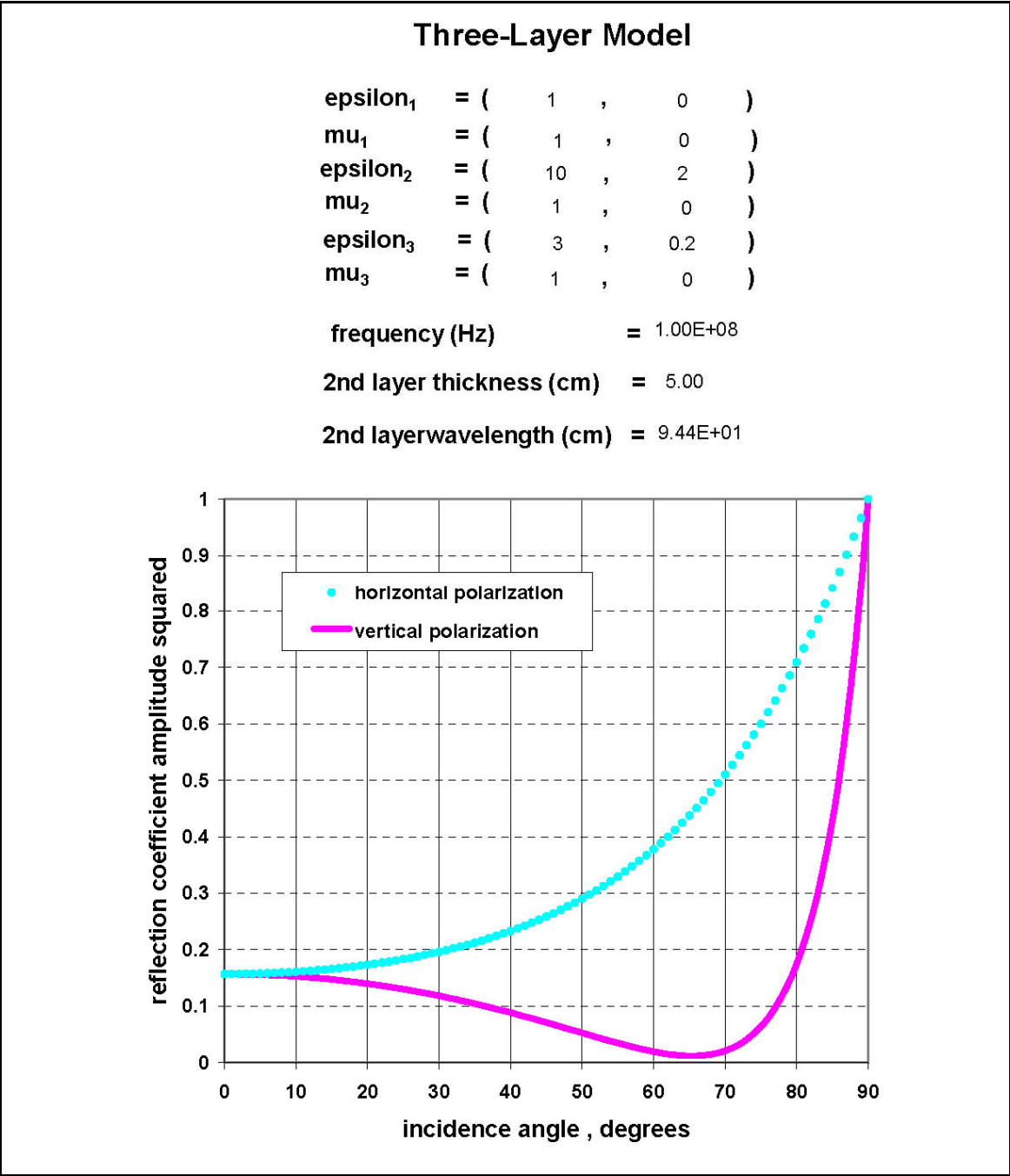


Figure 13. Reflectance from a thin, moist, moderately conductive soil layer over dry soil

different for the two cases, as is the value of the Brewster angle. The answer, then, is “Yes!” There must be significant penetration of the thin layer to produce such differences.

Fortunately, the computational tool has the means to determine how thick a layer must be before it appears to behave like a half-space. Figures 14 through 16 show reflectance values as a function of layer thickness at three different incident angles. Clearly, for the properties chosen, the moist layer would have to be very thick, probably on the order of three wavelengths, before it looked like a half-space. Note, also, the divergence of the polarized reflectances at higher values of incidence angles. Horizontally polarized waves become more reflective, while vertically polarized waves become less reflective.

A Growing Layer of Moist Soil Over Dry Soil

Another question that needs to be resolved through research is “If soil layer thickness makes a difference on reflectance values, is there another measurement parameter that could be related to only the material properties?” The rationale for this question lies with the fact that one may want to use ground-penetrating radar technology to measure soil properties such as moisture content. Moisture content is clearly a strong function of the soil’s dielectric properties (Curtis 2001), but for the simulations reported above, dielectric properties were not the only parameters that controlled the response to the signal. Layer thickness made a huge difference.

As a result of these observations, the computational tool was exercised to simulate a growing layer of moist soil over dry soil. Some of the results of these simulations are shown in Figures 17 to 21, which show reflectance vs incidence angle for top-layer thicknesses of 0, 5, 10, 15, and 20 cm. It is obvious that measurement results would be different for each increment of top-layer thickness. It is not obvious, however, that there is any one measurement parameter that remains fixed for all layer thicknesses. That would have to be the case in order for top-layer dielectric properties to be measurable for any layer thickness. (As an aside, one can see the change in the reflectance curves in a cartoon-like manner by displaying the tab entitled “power reflectance (3 layers)” while executing the tool’s macro.)

The most obvious measurement parameters that could possibly be used to infer dielectric properties would be normal incidence reflectance and the Brewster angle. Previous results (Figure 14) have already shown that normal incidence reflectance oscillates with layer thickness, and the cartoon simulation noted in the previous paragraph shows that the Brewster angle also moves around with changing layer thickness. As final proof of the latter observation, simulations were performed for 1-cm increments of thickness all the way to a top layer of 50 cm, which is a little over a half wavelength of material. Normal incidence reflectance values and Brewster angle values were hand tabulated

Specular Reflectance from Layered Materials

incidence angle (deg) = 0
frequency (Hz) = 1.00E+08
top layer wavelength (cm) = 9.44E+01
top layer dielectric constant = (10 , 2)
bottom layer dielectric constant = (3 , 0.2)

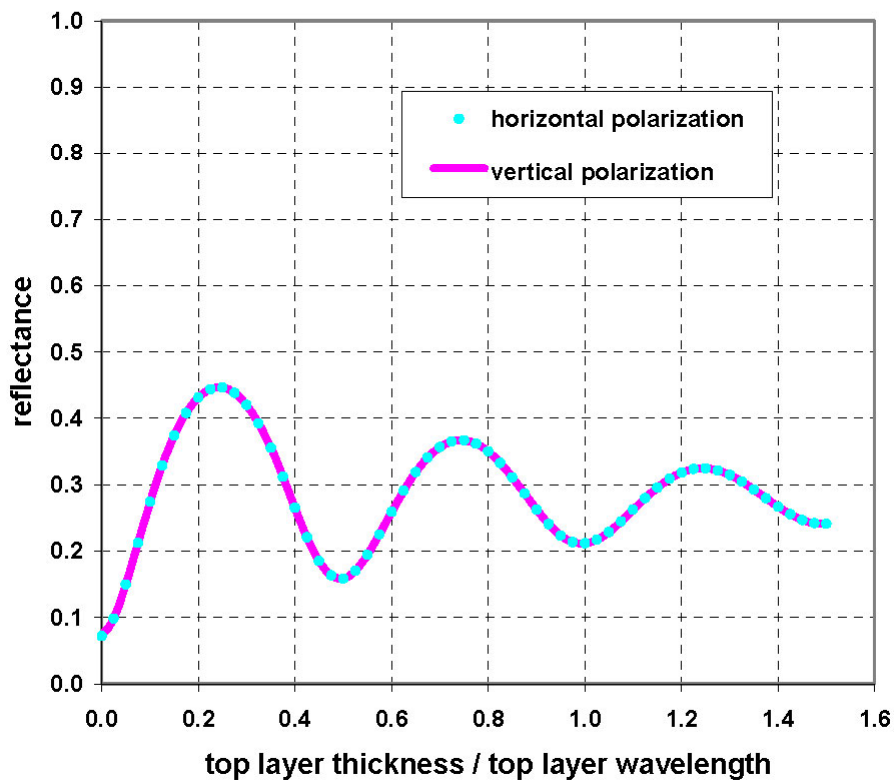


Figure 14. Layered soil reflectance vs top-layer thickness at normal incidence

Specular Reflectance from Layered Materials

incidence angle (deg) = 30
frequency (Hz) = 1.00E+08
top layer wavelength (cm) = 9.44E+01
top layer dielectric constant = (10 , 2)
bottom layer dielectric constant = (3 , 0.2)

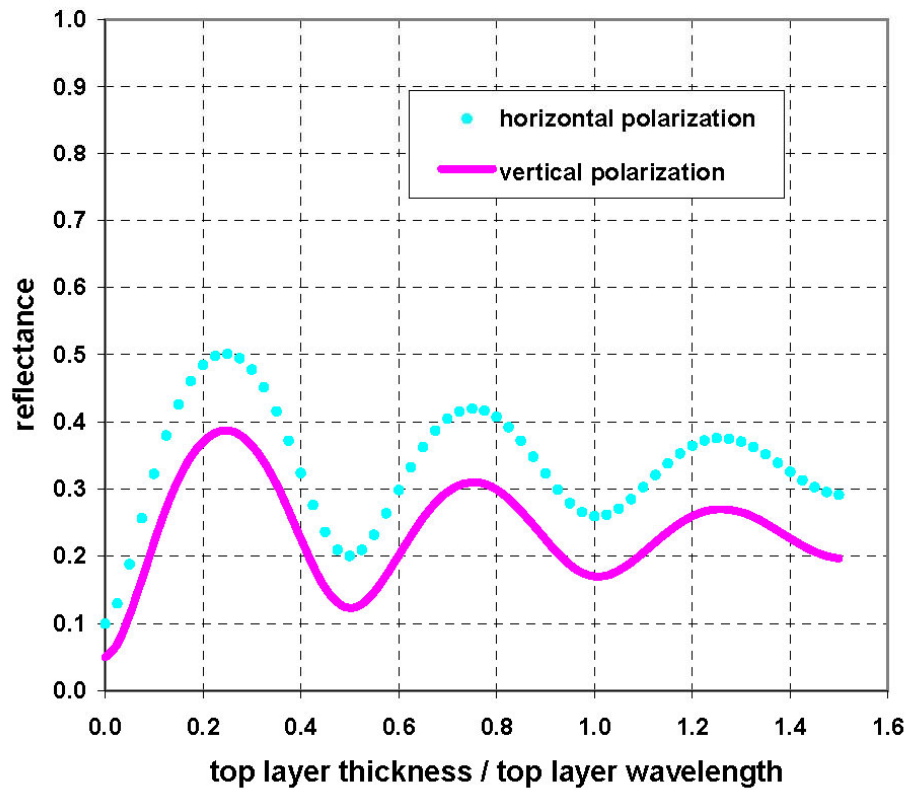


Figure 15. Layered soil reflectance vs top-layer thickness at 30 deg incidence

Specular Reflectance from Layered Materials

incidence angle (deg) = 60
frequency (Hz) = 1.00E+08
top layer wavelength (cm) = 9.44E+01
top layer dielectric constant = (10 , 2)
bottom layer dielectric constant = (3 , 0.2)

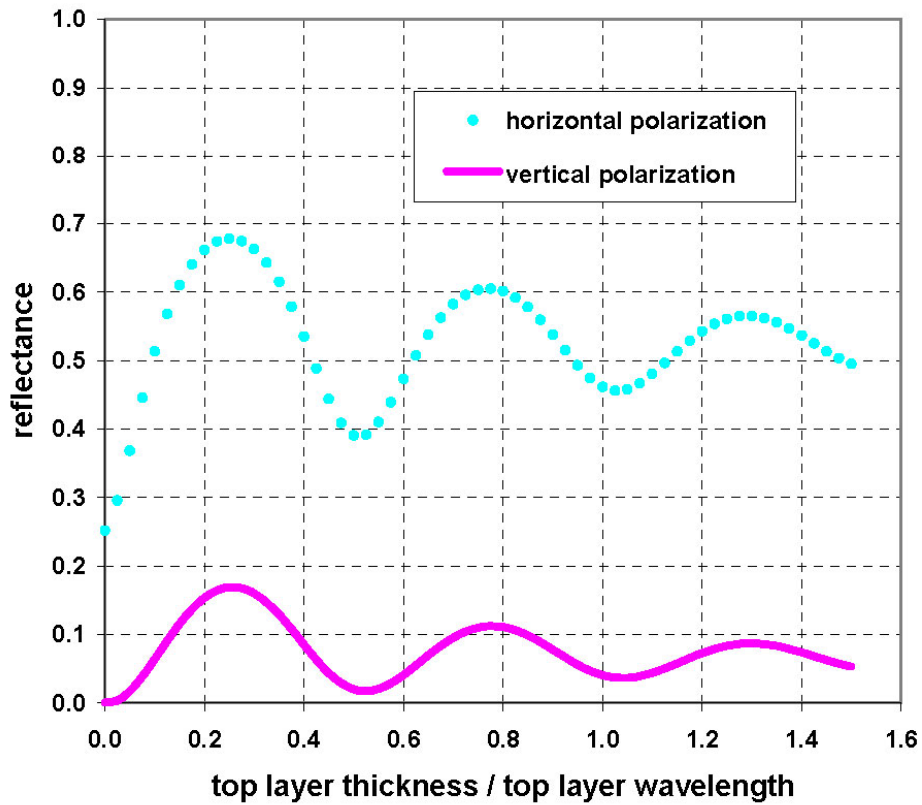


Figure 16. Layered soil reflectance vs top-layer thickness at 60 deg incidence

Three-Layer Model

$$\epsilon_{1} = (1 , 0)$$

$$\mu_{1} = (1 , 0)$$

$$\epsilon_{2} = (10 , 2)$$

$$\mu_{2} = (1 , 0)$$

$$\epsilon_{3} = (3 , 0.2)$$

$$\mu_{3} = (1 , 0)$$

$$\text{frequency (Hz)} = 1.00\text{E}+08$$

$$\text{2nd layer thickness (cm)} = 0.00$$

$$\text{2nd layer wavelength (cm)} = 9.44\text{E}+01$$

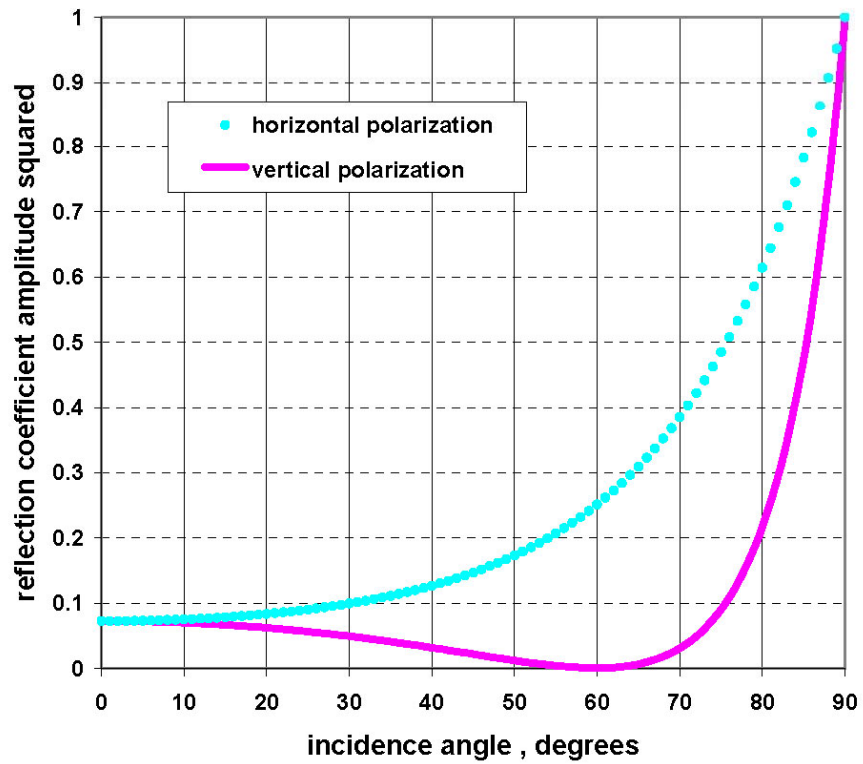


Figure 17. Reflectance from a dry soil half-space

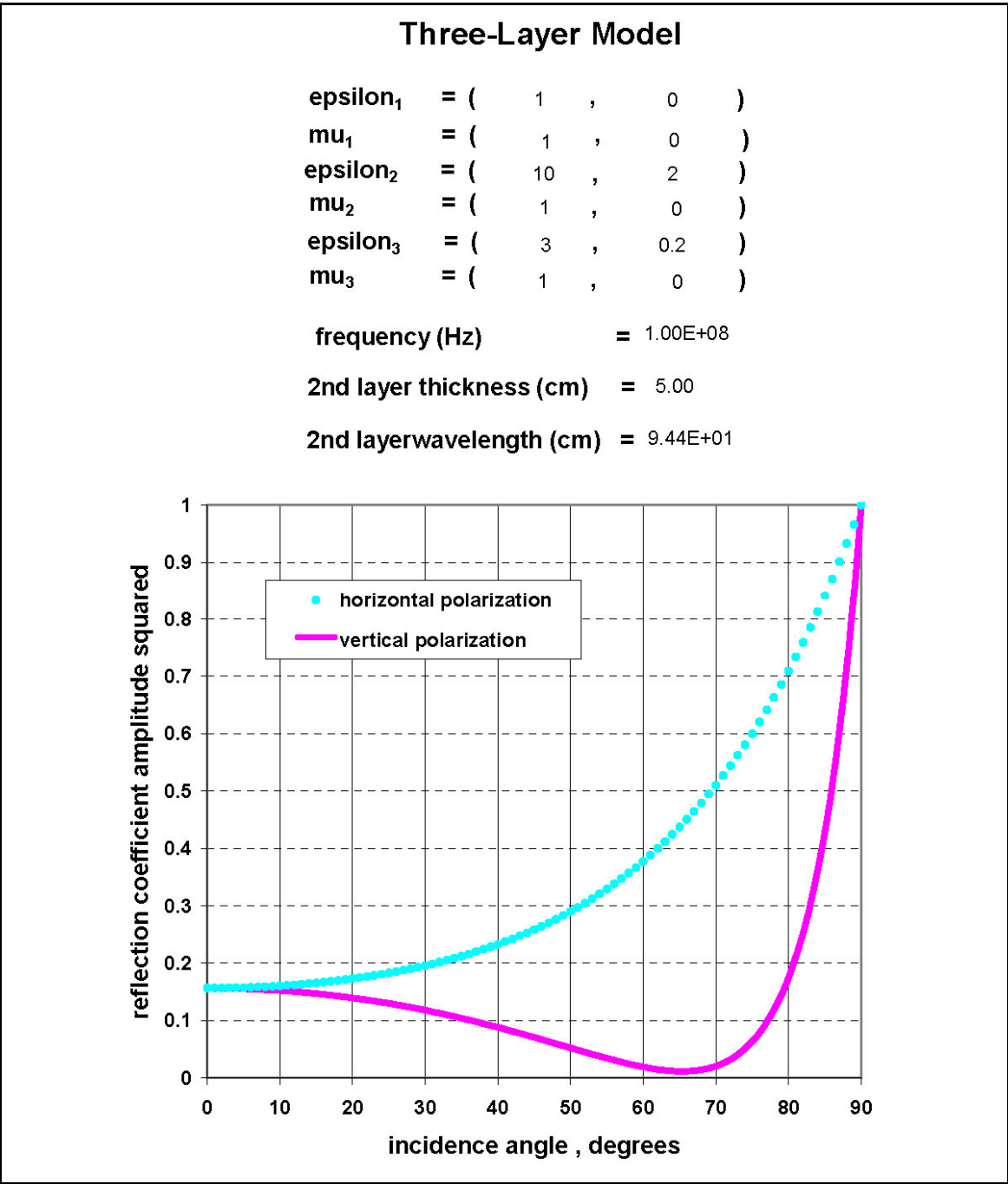


Figure 18. Reflectance from a 5-cm moist layer over a dry soil

Three-Layer Model

$$\epsilonpsilon_1 = (1 , 0)$$

$$\mu_1 = (1 , 0)$$

$$\epsilonpsilon_2 = (10 , 2)$$

$$\mu_2 = (1 , 0)$$

$$\epsilonpsilon_3 = (3 , 0.2)$$

$$\mu_3 = (1 , 0)$$

$$\text{frequency (Hz)} = 1.00\text{E}+08$$

$$\text{2nd layer thickness (cm)} = 10.00$$

$$\text{2nd layer wavelength (cm)} = 9.44\text{E}+01$$

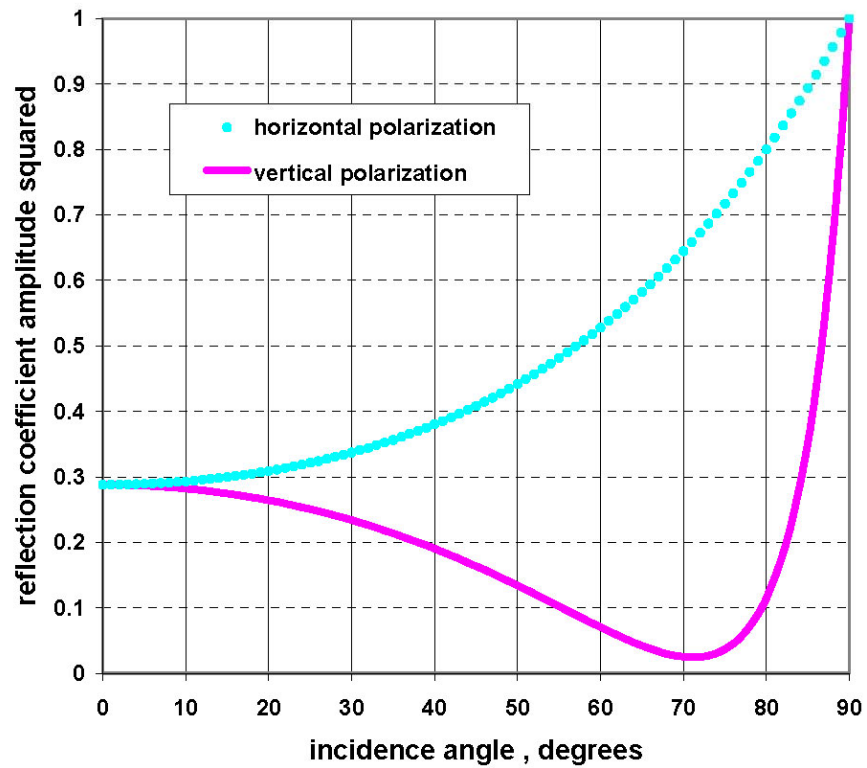


Figure 19. Reflectance from a 10-cm moist layer over a dry soil

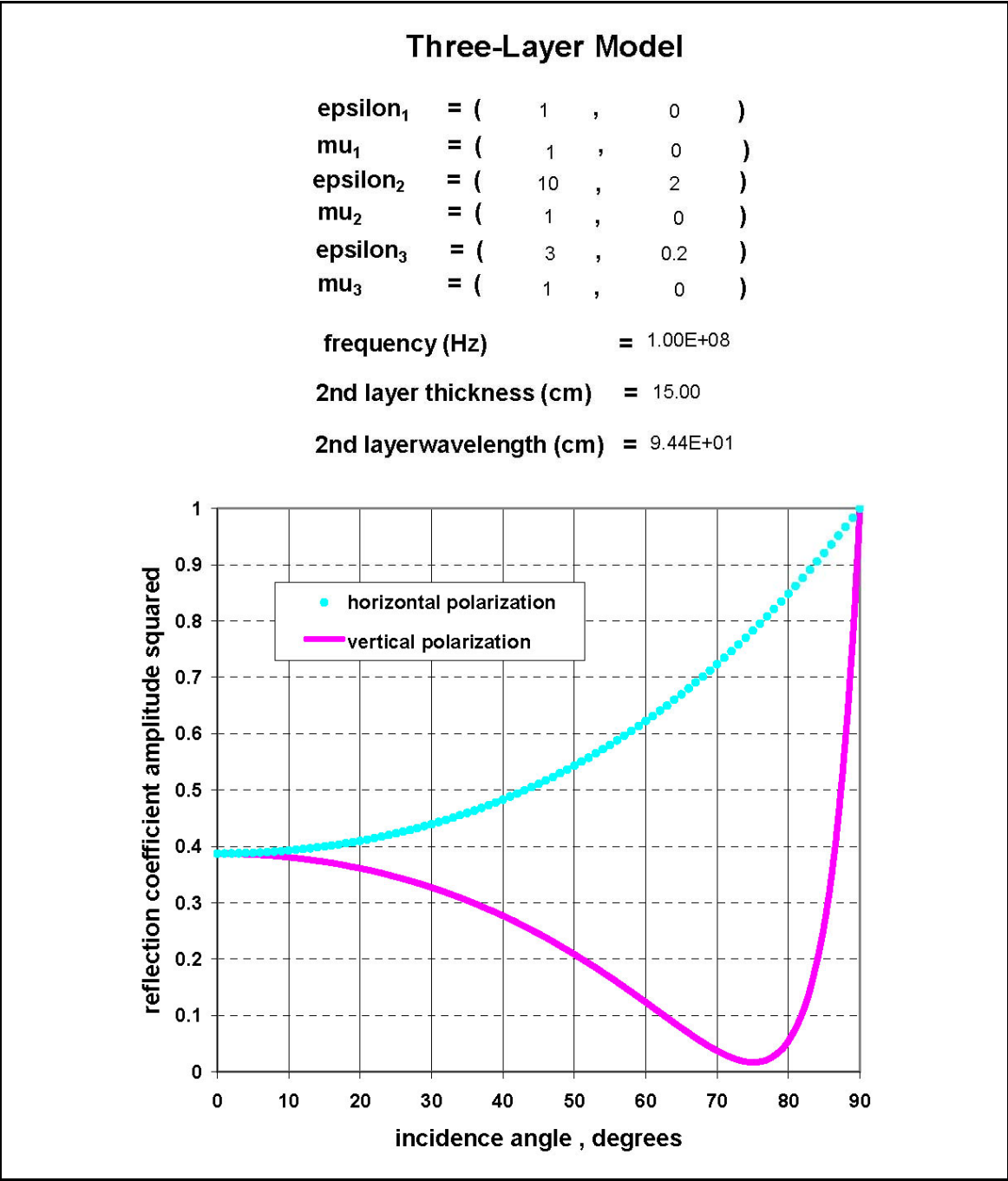


Figure 20. Reflectance from a 15-cm moist layer over a dry soil

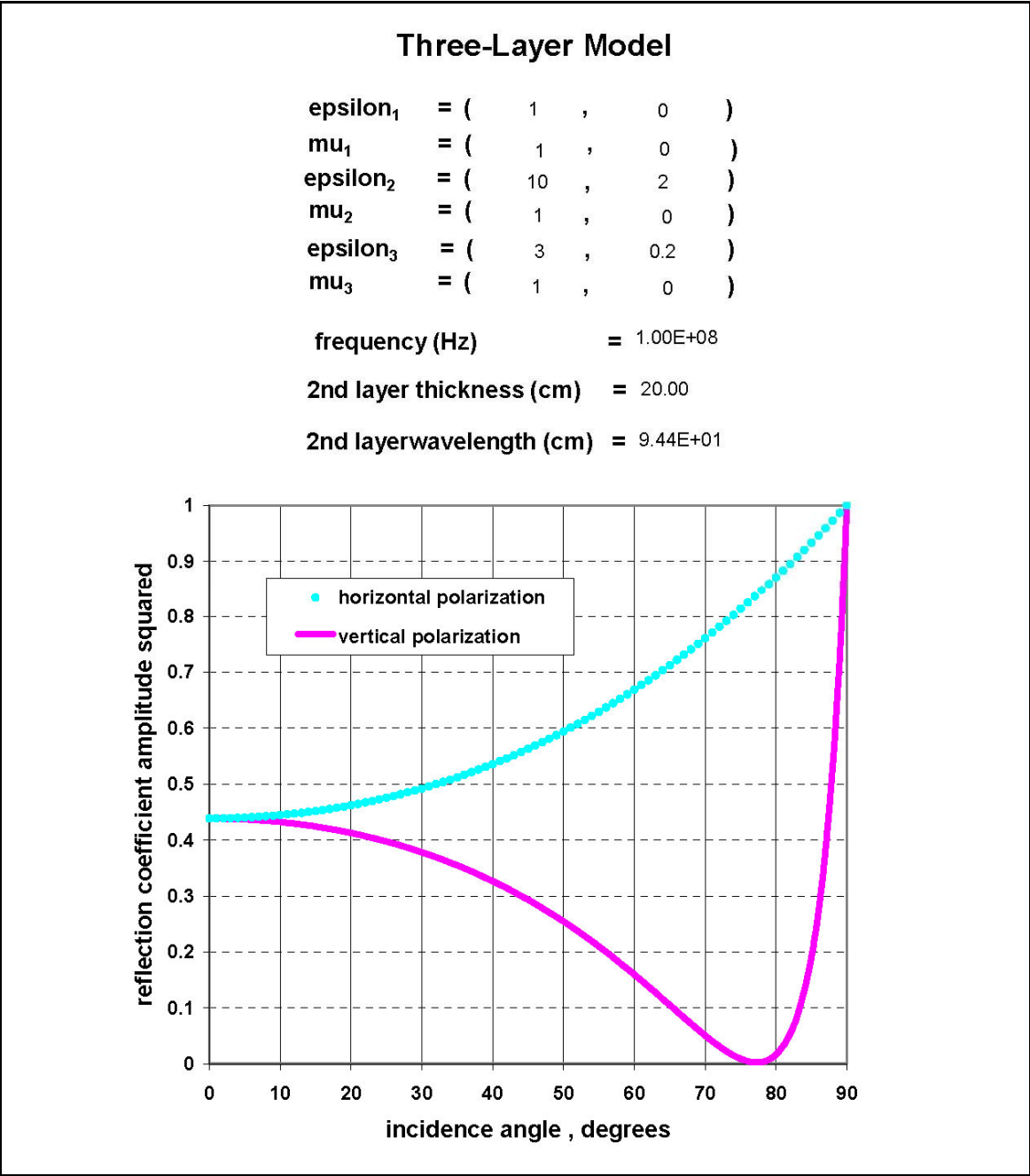


Figure 21. Reflectance from a 20-cm moist layer over a dry soil

and plotted on Figure 22. Clearly, Brewster angle tracks layer thickness in the same way that normal incidence reflectance does.

The final conclusion of this brief study is that as long as the layered structure of soil has an influence on the reflectance measurements that could be made from the soil, there does not appear to be a measurement that uniquely relates to dielectric properties, and thence to soil moisture. The only hope would be for higher frequency systems where the skin depth is much smaller or for measurements being made on highly conductive soils, which is the subject of the next section.

Low-Conductivity vs High-Conductivity Soils

The power of this computational tool is that it can be used to vary one parameter at a time to isolate the effects of that parameter on reflectance from soils. The first two sections in this chapter dealt with layer thickness as the variable. This section will look at electrical conductivity of the top soil layer as the primary variable of interest. What happens to reflectance measurements if the conductivity of the top layer changes by an order of magnitude?

Figures 23 through 25 are simulation results for a moist soil layer over a dry soil layer. Conductivity in the moist layer was taken to be 5 mS/m. Simulations for normal incidence, as well as 30 and 60 deg of incidence angle reveal a behavior similar to that of the previous section. Layer thickness is a dominant controlling factor, and polarized signal reflectances diverge for nonzero incidence angles.

When the conductivity of the top soil layer was taken to be an order of magnitude larger (50 mS/m), results changed dramatically. As seen in Figures 26 through 28, top-layer thickness becomes much less of a factor (the skin depth is much smaller). In fact, reflectance values settle into half-space results for less than a wavelength of top-layer thickness. The second observation to be noted is that the half-space reflectance appears to be about 20-percent higher for the high-conductivity soil than it is for the low-conductivity soil.

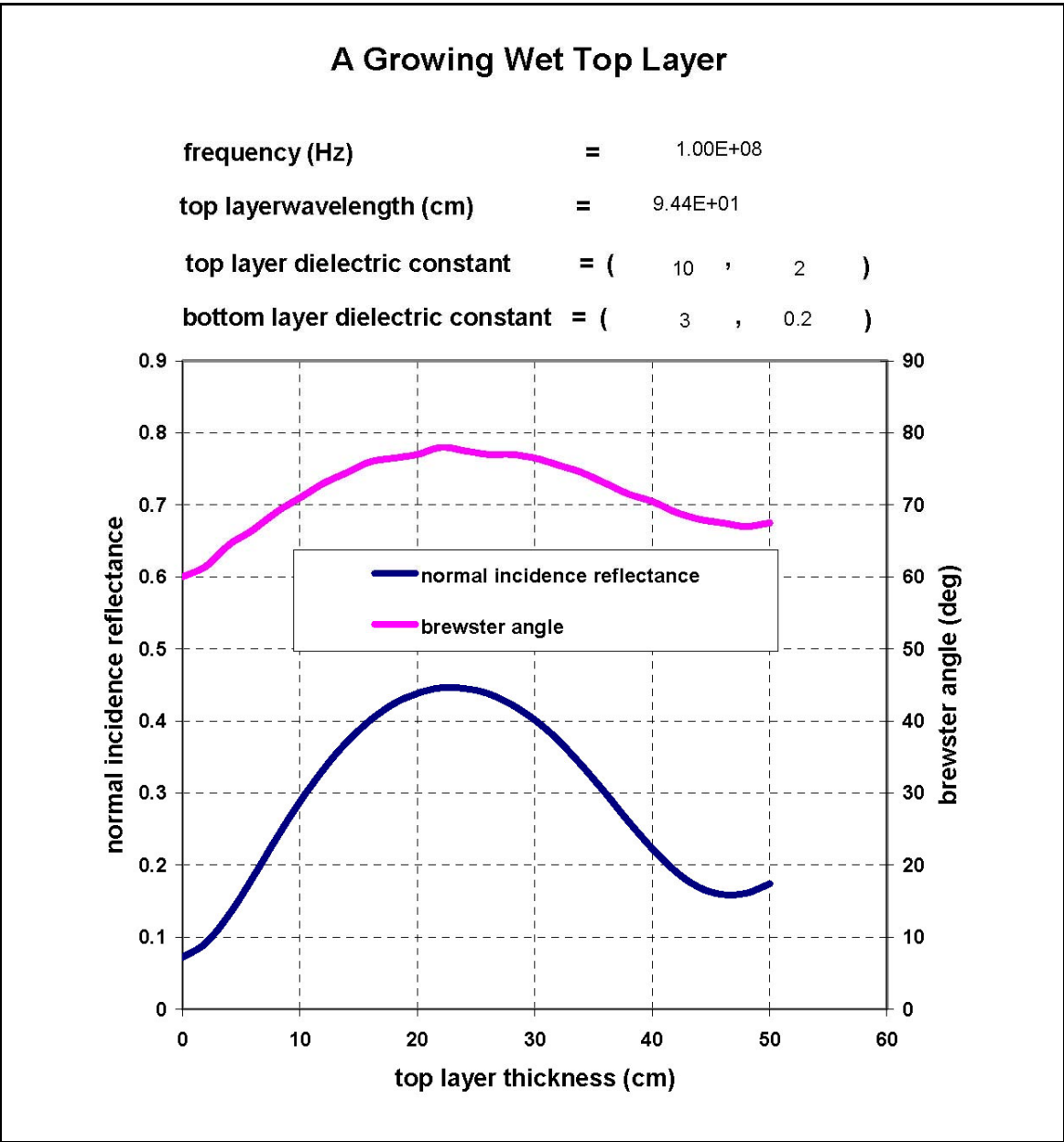


Figure 22. Impact of a growing moist soil layer on normal incidence reflectance and Brewster's angle

Specular Reflectance from Layered Materials

incidence angle (deg) = 0
frequency (Hz) = 1.00E+08
top layer wavelength (cm) = 9.48E+01
top layer dielectric constant = (10 , 0.9)
bottom layer dielectric constant = (3 , 0.2)

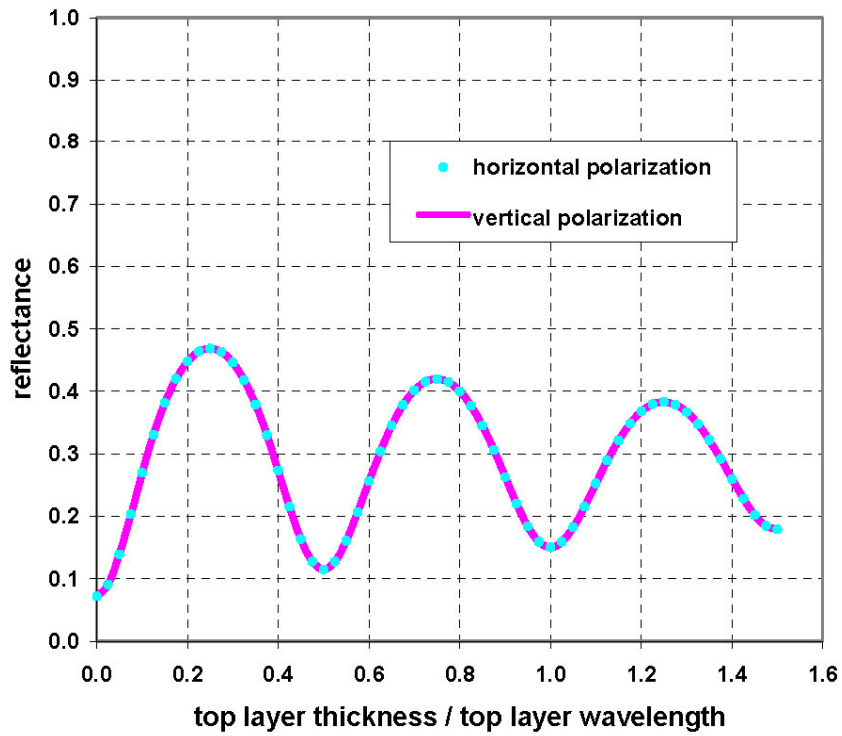


Figure 23. Reflectance from a low-loss moist layer at normal incidence

Specular Reflectance from Layered Materials

incidence angle (deg) = 30
frequency (Hz) = 1.00E+08
top layer wavelength (cm) = 9.48E+01
top layer dielectric constant = (10 , 0.9)
bottom layer dielectric constant = (3 , 0.2)

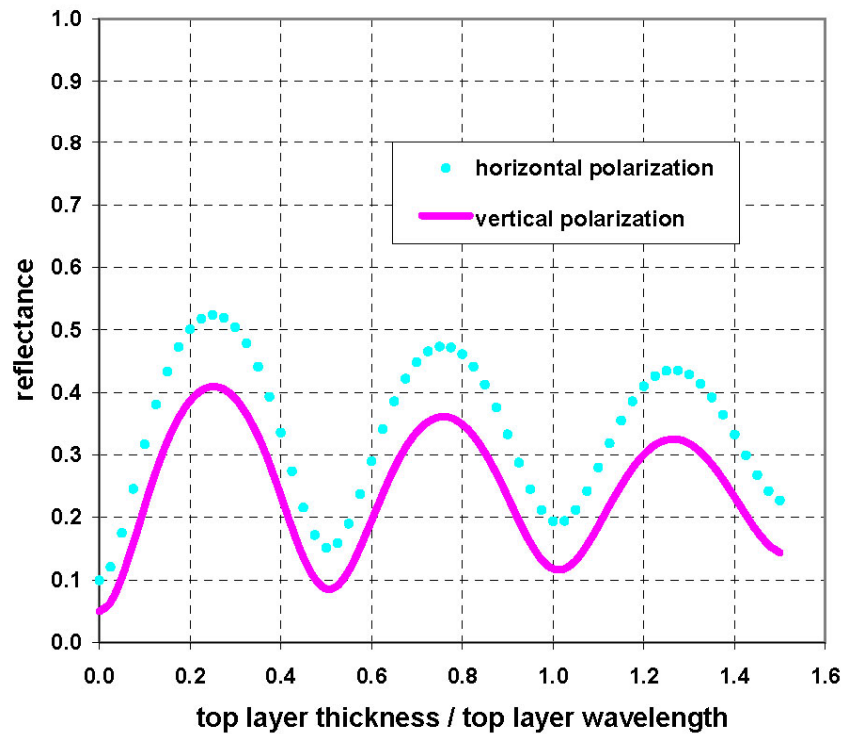


Figure 24. Reflectance from a low-loss moist layer at an incidence angle of 30 deg

Specular Reflectance from Layered Materials

incidence angle (deg) = 60
frequency (Hz) = 1.00E+08
top layer wavelength (cm) = 9.48E+01
top layer dielectric constant = (10 , 0.9)
bottom layer dielectric constant = (3 , 0.2)

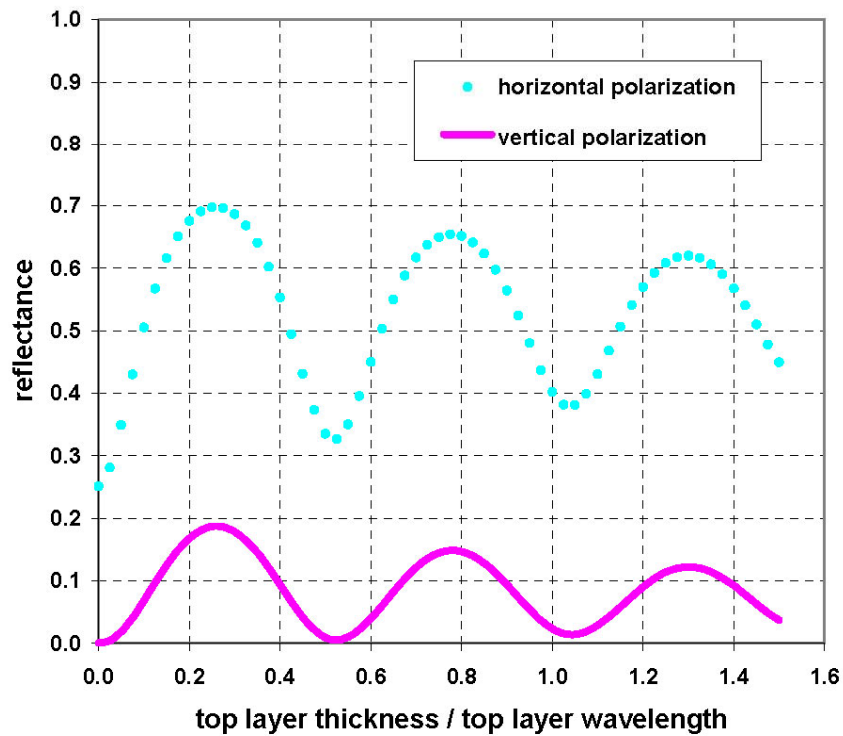


Figure 25. Reflectance from a low-loss moist layer at an incidence angle of 60 deg

Specular Reflectance from Layered Materials

incidence angle (deg) = 0
frequency (Hz) = 1.00E+08
top layer wavelength (cm) = 8.76E+01
top layer dielectric constant = (10 , 9)
bottom layer dielectric constant = (3 , 0.2)

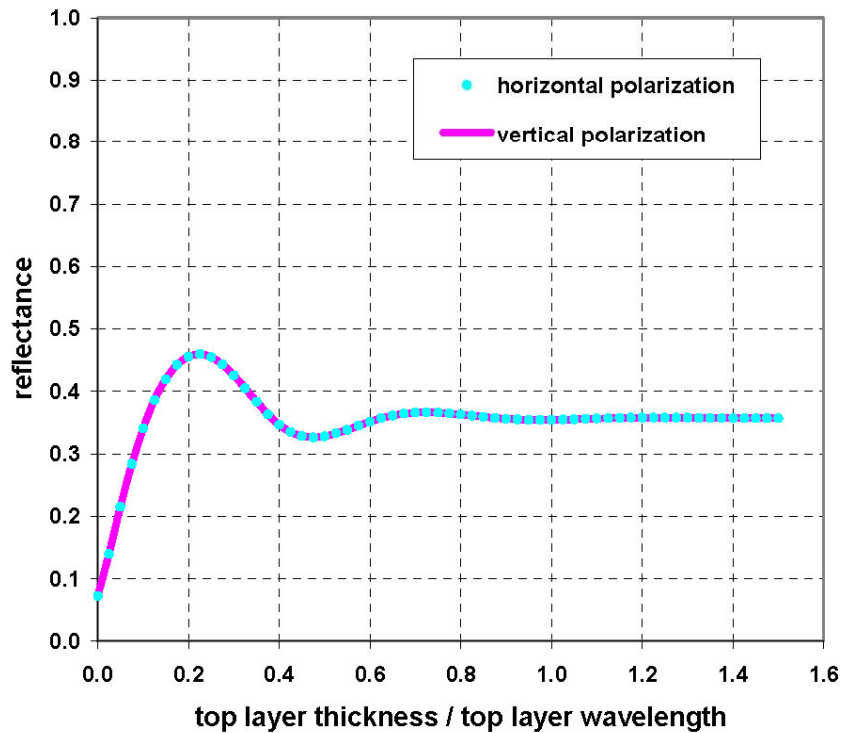


Figure 26. Reflectance from a high-loss moist layer at normal incidence

Specular Reflectance from Layered Materials

incidence angle (deg) = 30
frequency (Hz) = 1.00E+08
top layer wavelength (cm) = 8.76E+01
top layer dielectric constant = (10 , 9)
bottom layer dielectric constant = (3 , 0.2)

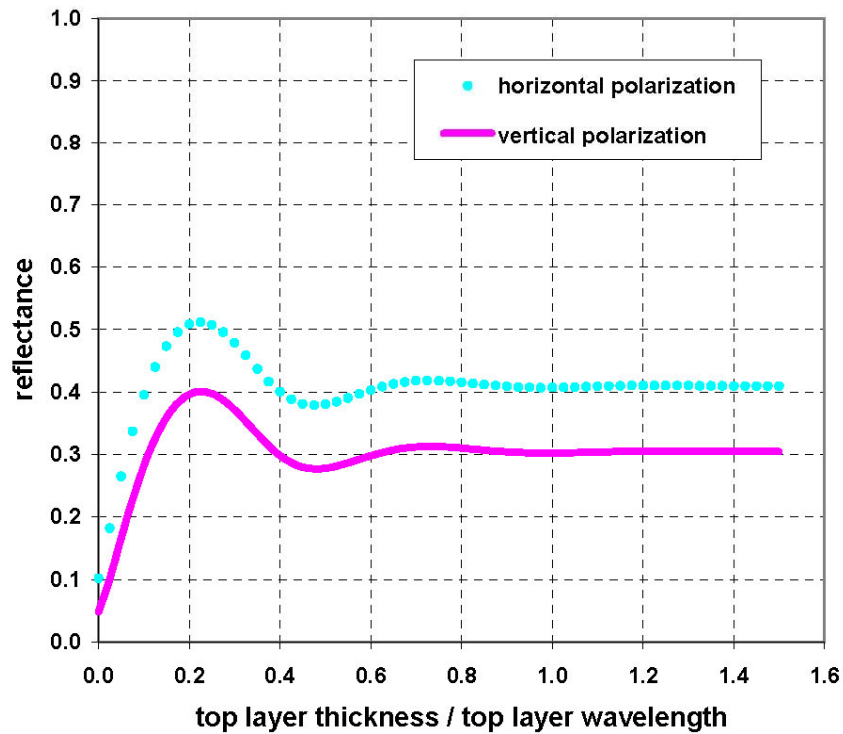


Figure 27. Reflectance from a high-loss moist layer at an incidence angle of 30 deg

Specular Reflectance from Layered Materials

incidence angle (deg) = 60
frequency (Hz) = 1.00E+08
top layer wavelength (cm) = 8.76E+01
top layer dielectric constant = (10 , 9)
bottom layer dielectric constant = (3 , 0.2)

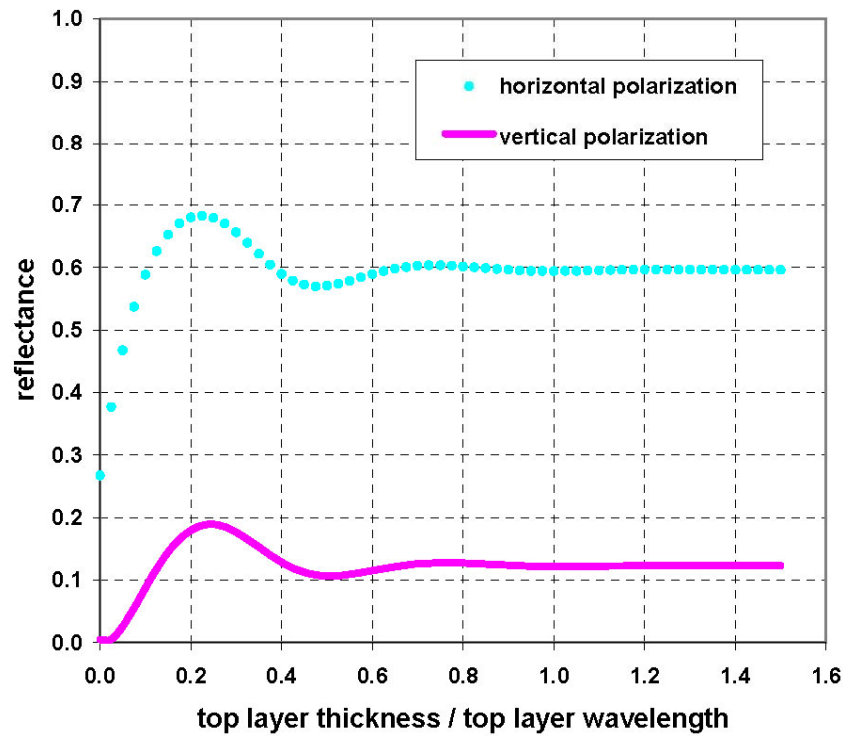


Figure 28. Reflectance from a high-loss moist layer at an incidence angle of 60 deg

5 Summary and Conclusions

The objective of this project was to develop a computational tool that would allow one to easily visualize radar reflection coefficients for a two-layered soil as a function of incidence angle. Input parameters should include radar frequency, top-layer thickness, and the complex dielectric properties of both soil layers. Such a tool can be used to conduct parametric studies that show the effect of top layer thickness and soil properties on radar reflectance values and Brewster angles.

An Excel file was created, a copy of which can be obtained from the author, that calculates the magnitude and phase of various reflection and transmission coefficients as well as the intensity of reflected energy (the magnitude squared) for any given layer properties and radar frequency. The validity of the tool was demonstrated by reproducing analytical solutions for layered media that can be found in numerous electromagnetics textbooks. Additional simulations were performed that addressed some very specific situations including the effect of a growing layer of moist soil and the impact of different soil conductivity values.

One of the benefits of this tool could be to help solve the inverse problem of deriving soil moisture values from measured radar reflectance data. For example, one could begin with the assumption that a particular patch of soil is well-approximated by a half-space geometry. Usually one has normal incidence reflectance measurements from that soil. The computational tool could be iteratively executed to find the complex dielectric constant of the soil that best matches the measured reflectance value. If one already has the relationship between volumetric soil moisture content and the complex dielectric properties of that soil, then a prediction of the volumetric soil moisture can be made.

Normally, however, soils are seldom well-approximated by a half-space geometry. This is particularly true in electromagnetic phenomena, where the electrical properties of the medium are so dependent on moisture values. The tool developed in this study gives the user a means of simulating more realistic soil environments. For example, soils are never uniformly moist. Soon after significant rainfall, soils that exhibit low permeability (such as clays) may be better approximated as a two-layer half space, where a wet top layer has much different dielectric properties than does the underlying drier soil. Reflectance values from the surface of the soil will be a function of the amount of moisture and the thickness of that top layer.

Another potential solution to the field measurement of soil moisture might be to develop a device for measuring the Brewster angle (or, at least the angle of minimum reflectance) of the soil using a relatively simple bistatic radar. Again, this computational tool could be used to help solve the inverse problem of relating Brewster angle values to soil moisture content.

References

- Arcone, S. A., and Larson, R. W. (1988). "Single-horn reflectometry in *in situ* dielectric measurements at microwave frequencies," *Communication, IEEE Transactions on Geoscience and Remote Sensing* 26(1), 89-92.
- Caldecott, R., Poirier, M., and Svoboda, D. E. (1985). "A radio frequency probe to measure soil electrical parameters," Final Report 715616-4, The Ohio State University, Columbus, OH.
- Campbell Scientific, Inc. (2004). "Water content reflectometer, Model CS616-L," Web site brochure.
- Curtis, J. O. (2001). "Moisture effects on the dielectric properties of soils," *IEEE Transactions on Geoscience and Remote Sensing* 39(1), 125-128.
- _____. (2004). "EM Power attenuation in soils," in preparation, U.S. Army Engineer Research and Development Center, Vicksburg, MS.
- Dobson, M. C., and Ulaby, F. T. (1986). "Active microwave soil moisture research," *IEEE Transactions on Geoscience and Remote Sensing* GE-24(1), 23-36.
- Dynamax, Inc. (2004). "TH₂O soil moisture meter," Web site brochure.
- Griffiths, D. J. (1981). *Introduction to electrodynamics*. Prentice-Hall, Inc., Englewood Cliffs, NJ.
- Jackson, J. D. (1975). *Classical electrodynamics*. John Wiley & Sons, New York.
- Klein, M. V., and Furtak, T. E. (1986). *Optics*. John Wiley & Sons, New York.
- Long, M. W. (1983). *Radar reflectivity of land and sea*. Artech House, Norwood, MA.
- Lundien, J. R. (1972). "Determining presence, thickness, and electrical properties of stratified media using swept-frequency radar," Technical Report M-72-4, U.S. Army Engineer Waterways Experiment Station, Vicksburg, MS.

- Reitz, J. R., Milford, F. J., and Christy, R. W. (1979). *Foundations of electromagnetic theory*. Addison-Wesley, Reading, MA.
- Schmugge, T. (1989). "Microwave remote sensing of soil moisture." *Applications of remote sensing to agrometeorology*, F. Toselli, ed, 257-284.
- Schey, H. M. (1973). *Div, grad, curl, and all that*. W. W. Norton & Co., New York.
- Stratton, J. B. (1941). *Electromagnetic theory*. McGraw-Hill, New York.
- Telford, W. M. Geldart, L. P., Sheriff, R. E., and Keys, D. A. (1976). *Applied geophysics*. Cambridge University Press, Cambridge, UK.
- Topp, G. C., Davis, J. L., and Annan, A. P. (1980). "Electromagnetic determination of soil water content: measurements in coaxial transmission lines," *Water Resources Research* 16, 574-582.
- Ulaby, F. T., Cihlar, J., and Moore, R. K. (1974). "Active microwave measurement of soil water content." *Remote Sensing of Environment* 3, 185-203.
- Waite, W. P., Sadeghi, A. M., and Scott, H. D. (1984). "Microwave bistatic reflectivity dependence on the moisture content and matric potential of bare soil," *IEEE Transactions on Geoscience and Remote Sensing* GE-22(4), 394-405.

Appendix A

Reflection and Refraction at a Plane Interface

Although numerous electromagnetics and optics textbooks present outlines of reflection/refraction formula derivations, a formal documentation of the derivation is presented in this appendix that includes minor details often assumed to be common knowledge by other authors. Hopefully, the information presented here will answer any questions readers may have about assumptions attached to the models utilized in this study. SI units are used throughout the text. The following draws heavily upon several sources (Jackson 1975; Reitz et al. 1979; Griffiths 1981; Schey 1973).¹

Maxwell's Equations

Based on experimental observations made during the early part of the 19th century, a set of field equations can be written that collectively describe the interactions among charges, currents, electric fields, and magnetic fields. Known as Maxwell's equations, because of a final contribution by the Scottish physicist James Clerk Maxwell in the latter part of the 19th century, they allow one to determine fields from known charges and currents as well as to predict the time-dependent evolution of fields given a known set of initial conditions. In differential form, one equation is referred to as Gauss's Law:

$$\bar{\nabla} \cdot \bar{D} = \rho \quad (\text{A1})$$

which relates how much the electric displacement field, \mathbf{D} , diverges (or spreads out) from a point to the charge density at that point, ρ . In integral form, this law associates the flux of the field through a volume of material to the free charge enclosed within that volume. A similar equation (having no named source) accounts for the observation that a magnetic field, \mathbf{B} , does not derive from point sources:

¹ References cited in this appendix are located at the end of the main text.

$$\bar{\nabla} \cdot \bar{B} = 0 \quad (\text{A2})$$

The third equation, known as Faraday's Law, formalizes the observation that a time-varying magnetic field can induce an electric field, \bar{E} :

$$\bar{\nabla} \times \bar{E} = -\frac{\partial \bar{B}}{\partial t} \quad (\text{A3})$$

Finally, there is Maxwell's extension to Ampere's Law, which accounts for the fact that time-varying electric fields can induce magnetic fields in materials:

$$\bar{\nabla} \times \bar{H} = \sigma \bar{E} + \frac{\partial \bar{D}}{\partial t} \quad (\text{A4})$$

where current density has been taken to be linearly proportional to the electric field, and the constant of proportionality, σ , is the electrical conductivity of material.

The following constitutive properties relate the auxiliary magnetic field, \bar{H} , to the magnetic field, \bar{B} , and the electric displacement field, \bar{D} , to the electric field, \bar{E} :

$$\bar{H} = \frac{1}{\mu} \bar{B} \quad (\text{A5})$$

and

$$\bar{D} = \epsilon \bar{E} \quad (\text{A6})$$

where μ is the magnetic permeability, and ϵ is the electrical permittivity of the material.

The Wave Equation

Assuming that there is no free charge in a volume of material, and assuming that material is linear (constitutive properties are all constants), a wave equation for the electric field can be derived in the following manner. First of all, apply the curl operator to Faraday's Law:

$$\bar{\nabla} \times \bar{\nabla} \times \bar{E} = -\bar{\nabla} \times \frac{\partial \bar{B}}{\partial t}$$

Then use Ampere's Law to eliminate the magnetic field term:

$$\bar{\nabla} \times \bar{\nabla} \times \bar{E} = -\mu\sigma \frac{\partial \bar{E}}{\partial t} - \mu\epsilon \frac{\partial^2 \bar{E}}{\partial t^2}$$

The operator on the left-hand side of the last equation can be replaced by the vector identity:

$$\bar{\nabla} \times \bar{\nabla} \times = \bar{\nabla} \bar{\nabla} \cdot - \nabla^2$$

The final result is a wave equation for electric fields that has an added term because of the conductivity of the material:

$$\nabla^2 \bar{E} - \mu\sigma \frac{\partial \bar{E}}{\partial t} - \mu\epsilon \frac{\partial^2 \bar{E}}{\partial t^2} = 0 \quad (\text{A7})$$

Electric Field and Magnetic Field Solutions

For monochromatic waves, the generalized solution to the wave equation is:

$$\bar{E}(\bar{r}, t) = \bar{E}_0 e^{i(\bar{k} \cdot \bar{r} - \omega t)} \quad (\text{A8})$$

where the magnitude of the wave vector (in the direction of propagation) is the wave number:

$$k \equiv \frac{2\pi}{\lambda} = \frac{2\pi f}{v} = \frac{\omega}{v} = \frac{N\omega}{c} \quad (\text{A9})$$

N is the index of refraction of the material, ω is the radial frequency of the sinusoidal wave, v is the wave speed in the material, and c is the speed of light in free space. Substituting the solution into the wave equation gives the relationship among the material properties, the wave number, and the index of refraction:

$$k^2 = \mu\epsilon\omega^2 + i\mu\sigma\omega = \frac{N^2\omega^2}{c^2} \quad (\text{A10})$$

or

$$N^2 = \mu\epsilon c^2 + i \frac{\mu\sigma c^2}{\omega} = \hat{K} = K_r + iK_i \quad (\text{A11})$$

Therefore, the index of refraction is complex and, in turn, defines a complex dielectric constant whose real part is:

$$K_r = \mu \epsilon c^2 = \frac{\mu \epsilon}{\mu_0 \epsilon_0} \quad (\text{A12})$$

and whose imaginary part is:

$$K_i = \frac{\mu \sigma}{\mu_0 \epsilon_0 \omega} \quad (\text{A13})$$

where μ_0 is the magnetic permeability of free space ($4\pi \times 10^{-7}$ newton/ampere²), and ϵ_0 is the electrical permittivity of free space (8.85×10^{-12} coulomb²/newton-meter²). For the vast majority of materials, the magnetic permeability is a number whose value is very, very close to that of free space. Only a few minerals in soils, such as ilmenite and magnetite (Telford et al. 1976) have significant values of permeability. In almost all cases, then, one can ignore the ratio of μ/μ_0 in the definition of the complex dielectric constant.

Given the solution (Equation A8) to the wave equation for electric fields (Equation A7), one can easily find the solution for the corresponding magnetic field by making use of Faraday's Law. First of all, one must recognize that

$$\vec{k} \cdot \vec{r} = k_x x + k_y y + k_z z \quad (\text{A14})$$

Then

$$\frac{\partial \vec{E}}{\partial x} = \vec{E}_0 e^{i(\vec{k} \cdot \vec{r} - \omega t)} \frac{\partial (i\vec{k} \cdot \vec{r})}{\partial x} = ik_x \vec{E} \quad (\text{A15})$$

Similar terms for the y and z partial derivatives yield the useful relationship that

$$\vec{\nabla} = i\vec{k}, \quad (\text{A16})$$

or that the left-hand side of Faraday's Law becomes:

$$\vec{\nabla} \times \vec{E} = i\vec{k} \times \vec{E} \quad (\text{A17})$$

Therefore, the magnetic field must be proportional to the cross product of the wave vector and the electric field.

As for the right-hand side of Faraday's Law, one can assume that the magnetic field has a generalized solution like Equation A8 and, therefore,

$$-\frac{\partial}{\partial t} = i\omega \quad (\text{A18})$$

Substituting Equations A16 and A18 into Equation A3 finally yields:

$$\vec{B} = \frac{1}{\omega} \vec{k} \times \vec{E} = \frac{k}{\omega} \hat{k} \times \vec{E} = \frac{N}{c} \hat{k} \times \vec{E} = \frac{1}{v} \hat{k} \times \vec{E} \quad (\text{A19})$$

where \hat{k} is the unit vector in the direction of wave propagation.

Reflection and Refraction Fields

Following the notation shown in Figure A1, one may now write expressions for the incident, reflected, and refracted electric and magnetic fields:

Incident fields

$$\vec{E}_I = \vec{E}_{I0} e^{i(\vec{k}_I \cdot \vec{r} - \omega t)} \quad \vec{B}_I = \frac{1}{\omega} \vec{k}_I \times \vec{E}_I \quad (\text{A20})$$

Reflected fields

$$\vec{E}_R = \vec{E}_{R0} e^{i(\vec{k}_R \cdot \vec{r} - \omega t)} \quad \vec{B}_R = \frac{1}{\omega} \vec{k}_R \times \vec{E}_R \quad (\text{A21})$$

Refracted fields

$$\vec{E}_T = \vec{E}_{T0} e^{i(\vec{k}_T \cdot \vec{r} - \omega t)} \quad \vec{B}_T = \frac{1}{\omega} \vec{k}_T \times \vec{E}_T \quad (\text{A22})$$

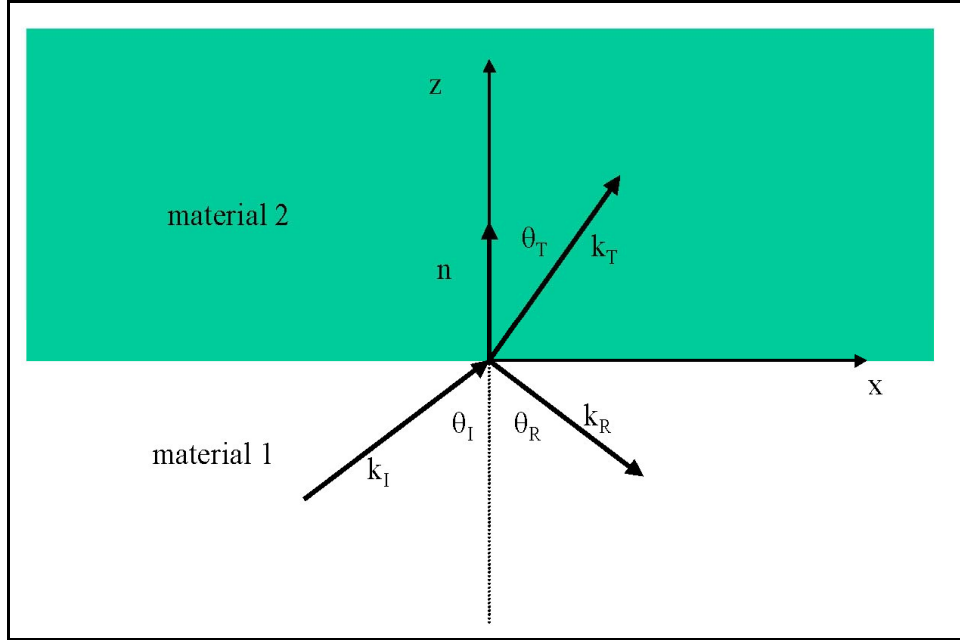


Figure A1. Incident (k_I), reflected (k_R), and refracted (k_T) waves at a plane interface

The magnitudes of the wave vectors are just:

$$|\vec{k}_I| = |\vec{k}_R| = k_1 = \frac{N_1\omega}{c} \text{ and } |\vec{k}_T| = k_2 = \frac{N_2\omega}{c} \quad (\text{A23})$$

Boundary Conditions

Before applying boundary conditions to the field equations, consider the benefits of the assumption that at any instant of time on the interface boundary ($z = 0$), the incident wave instantaneously generates reflected and refracted waves having the same frequency. In other words, all three waves have the same phase at that instant of time. In terms of the wave vectors:

$$(\vec{k}_I \cdot \vec{r})_{z=0} = (\vec{k}_R \cdot \vec{r})_{z=0} = (\vec{k}_T \cdot \vec{r})_{z=0} \quad (\text{A24})$$

Having no reason to believe that the three wave vectors are not all in the plane of incidence (y-components are zero, and given that $z = 0$ at the boundary, then the phase constraint means that the x-component of each wave vector is identical at the boundary. In other words,

$$k_I \sin \theta_I = k_R \sin \theta_R = k_T \sin \theta_T \quad (\text{A25})$$

Since $k_I = k_R = k_T$, the incidence angle must then equal the reflection angle, which we can call θ_I . Furthermore, one can now relate the incidence angle and the transmission angle through Snell's law:

$$\frac{\sin \theta_1}{\sin \theta_2} = \frac{k_2}{k_1} = \frac{N_2}{N_1} \quad (\text{A26})$$

In order to derive expressions for the amplitudes of the reflected and refracted waves (for it is the wave amplitude that is detected by a receiver instrument), one must now apply boundary conditions for the electric and magnetic fields. Given that there are no preexisting free charges on the interface, nor are there any preexisting currents on the interface because of those charges, then in words one can state that the normal components of the electric displacement field, \mathbf{D} , and the magnetic field, \mathbf{B} , must be continuous across the interface, as are the tangential components of the electric field, \mathbf{E} , and the auxiliary magnetic field, \mathbf{H} . In equation form, the boundary conditions are:

$$[\varepsilon_1(\vec{E}_{I0} + \vec{E}_{R0}) - \varepsilon_2\vec{E}_{T0}] \cdot \hat{n} = 0 \quad (\text{A27})$$

$$[\vec{k}_I \times \vec{E}_{I0} + \vec{k}_R \times \vec{E}_{R0} - \vec{k}_T \times \vec{E}_{T0}] \cdot \hat{n} = 0 \quad (\text{A28})$$

$$[\vec{E}_{I0} + \vec{E}_{R0} - \vec{E}_{T0}] \times \hat{n} = 0 \quad (\text{A29})$$

$$\left[\frac{1}{\mu_1} (\bar{k}_I \times \bar{E}_{I0} + \bar{k}_R \times \bar{E}_{R0}) - \frac{1}{\mu_2} (\bar{k}_T \times \bar{E}_{T0}) \right] \times \hat{n} = 0 \quad (\text{A30})$$

Amplitude Reflection and Transmission (Refraction) Coefficients

Because any incident electric field vector can be defined by two orthogonal vectors, amplitude reflection and refraction coefficients (ratios) will be developed for two special cases: one in which the electric field is normal to the plane of incidence (horizontal polarization), and one in which the field lies within the plane of incidence (vertical polarization).

Horizontal polarization

For this special case, the field amplitude vectors and wave propagation vectors take on the following forms:

$$\bar{E}_{I0} = E_{I0} \hat{j}, \quad \bar{E}_{R0} = E_{R0} \hat{j}, \quad \bar{E}_{T0} = E_{T0} \hat{j} \quad (\text{A31})$$

$$\bar{k}_I = k_1 \sin \theta_1 \hat{i} + k_1 \cos \theta_1 \hat{k} \quad (\text{A32})$$

$$\bar{k}_R = k_1 \sin \theta_1 \hat{i} - k_1 \cos \theta_1 \hat{k} \quad (\text{A33})$$

$$\bar{k}_T = k_2 \sin \theta_2 \hat{i} + k_2 \cos \theta_2 \hat{k} \quad (\text{A34})$$

Inserting these vector definitions into the first boundary condition, Equation A27, yields nothing. The second boundary condition, Equation A28, combined with Snell's law, yields the same relationship that one gets from the third boundary condition; namely:

$$E_{I0} + E_{R0} - E_{T0} = 0 \quad (\text{A35})$$

The fourth boundary condition, Equation A30, yields:

$$-\frac{k_1}{\mu_1} E_{I0} \cos \theta_1 + \frac{k_1}{\mu_1} E_{R0} \cos \theta_1 + \frac{k_2}{\mu_2} E_{T0} \cos \theta_2 = 0 \quad (\text{A36})$$

Equations A35 and A36 can be solved simultaneously to arrive at a reflection amplitude coefficient and a refraction amplitude coefficient. For example,

$$\frac{E_{R0}}{E_{I0}} = \frac{\cos \theta_1 - \frac{\mu_1 k_2}{\mu_2 k_1} \cos \theta_2}{\cos \theta_1 + \frac{\mu_1 k_2}{\mu_2 k_1} \cos \theta_2} \quad (\text{A37})$$

Known parameters will be the incidence angle and the optical properties of each layer. The transmission angle can be eliminated from Equation A37 by using both Snell's law and the trigonometric identity: $\sin^2 \theta + \cos^2 \theta = 1$. Furthermore, the wave number in each layer can be replaced by terms that include either the complex index of refraction or the complex dielectric constant defined by Equation A11:

$$\frac{E_{R0}}{E_{I0}} = \frac{\cos \theta_1 - \frac{\mu_1}{\mu_2} \sqrt{\frac{\widehat{K}_2}{\widehat{K}_1} - \sin^2 \theta_1}}{\cos \theta_1 + \frac{\mu_1}{\mu_2} \sqrt{\frac{\widehat{K}_2}{\widehat{K}_1} - \sin^2 \theta_1}} \quad (\text{A38})$$

Using Equations A12 and A13 to express the reflectance amplitude coefficient in terms of dielectric permittivity and electrical conductivity, one finally has:

$$\frac{E_{R0}}{E_{I0}} = \frac{\cos \theta_1 - \frac{\mu_1}{\mu_2} \sqrt{\left(\frac{\mu_2}{\mu_1} \right) \left(\frac{\frac{\varepsilon_2 + i \frac{\sigma_2}{\varepsilon_0}}{\varepsilon_0} + i \frac{\sigma_2}{\varepsilon_0 \omega}}{\frac{\varepsilon_1 + i \frac{\sigma_1}{\varepsilon_0}}{\varepsilon_0} + i \frac{\sigma_1}{\varepsilon_0 \omega}} \right) - \sin^2 \theta_1}}{\cos \theta_1 + \frac{\mu_1}{\mu_2} \sqrt{\left(\frac{\mu_2}{\mu_1} \right) \left(\frac{\frac{\varepsilon_2 + i \frac{\sigma_2}{\varepsilon_0}}{\varepsilon_0} + i \frac{\sigma_2}{\varepsilon_0 \omega}}{\frac{\varepsilon_1 + i \frac{\sigma_1}{\varepsilon_0}}{\varepsilon_0} + i \frac{\sigma_1}{\varepsilon_0 \omega}} \right) - \sin^2 \theta_1}} \quad (\text{A39})$$

Other authors report the same relationship shown in Equation A39, but usually express it in terms of a complex index of refraction. This author's recent body of work has exclusively dealt with measurements of the complex dielectric properties of soils under the assumption of nonmagnetic behavior. In that case the complex relative dielectric constant for layer 1 is just

$$\widehat{\varepsilon}_1 = \frac{\varepsilon_1}{\varepsilon_0} + i \frac{\sigma_1}{\varepsilon_0 \omega} = \varepsilon_1' + i \varepsilon_1'' \quad (\text{A40})$$

and Equation A39 can be expressed in the form inserted into the Excel file used to generate the reflection/refraction results shown in this report:

$$\frac{E_{R0}}{E_{I0}} = \frac{\cos \theta_1 - \frac{\mu_1}{\mu_2} \sqrt{\frac{\mu_2 \hat{\epsilon}_2}{\mu_1 \hat{\epsilon}_1} - \sin^2 \theta_1}}{\cos \theta_1 + \frac{\mu_1}{\mu_2} \sqrt{\frac{\mu_2 \hat{\epsilon}_2}{\mu_1 \hat{\epsilon}_1} - \sin^2 \theta_1}} \quad (\text{A41})$$

Combining Equations A35 and A41 yields the corresponding transmission (or refraction) amplitude coefficient:

$$\frac{E_{T0}}{E_{I0}} = \frac{2 \cos \theta_1}{\cos \theta_1 + \frac{\mu_1}{\mu_2} \sqrt{\frac{\mu_2 \hat{\epsilon}_2}{\mu_1 \hat{\epsilon}_1} - \sin^2 \theta_1}} \quad (\text{A42})$$

Vertical polarization

For the case of vertical polarization, all of the electric field vectors lie in the plane of incidence and take the forms:

$$\vec{E}_{I0} = -E_{I0} \cos \theta_1 \hat{i} + E_{I0} \sin \theta_1 \hat{k} \quad (\text{A43})$$

$$\vec{E}_{R0} = E_{R0} \cos \theta_1 \hat{i} + E_{R0} \sin \theta_1 \hat{k} \quad (\text{A44})$$

$$\vec{E}_{T0} = -E_{T0} \cos \theta_2 \hat{i} + E_{T0} \sin \theta_2 \hat{k} \quad (\text{A45})$$

The wave propagation vectors are identical to Equations A32 through A34.

Applying these vector definitions to the first boundary condition (Equation A27) yields an equation identical to that derived by applying the fourth boundary condition (Equation A30):

$$\frac{\vec{E}_{T0}}{\vec{E}_{I0}} = \sqrt{\frac{\mu_2 \hat{\epsilon}_1}{\mu_1 \hat{\epsilon}_2}} \left(1 + \frac{E_{R0}}{E_{I0}} \right) \quad (\text{A46})$$

In this case, all of the substitutions described above for the case of horizontal polarization have already been applied to derive the transmission amplitude coefficient in terms of the reflection amplitude coefficient.

The second boundary condition (Equation A28) provides nothing, while the third boundary condition (Equation A29) gives:

$$\frac{\vec{E}_{T0}}{\vec{E}_{I0}} = \frac{\cos \theta_1}{\cos \theta_2} \left(1 - \frac{E_{R0}}{E_{I0}} \right) \quad (\text{A47})$$

Setting Equation A46 equal to Equation A47 provides a formula for the reflection amplitude coefficient for vertical polarization in terms of layer properties and the angle of incidence:

$$\frac{E_{R0}}{E_{I0}} = \frac{\cos \theta_1 - \sqrt{\frac{\mu_2 \hat{\epsilon}_1}{\mu_1 \hat{\epsilon}_2} - \left(\frac{\hat{\epsilon}_1}{\hat{\epsilon}_2}\right)^2 \sin^2 \theta_1}}{\cos \theta_1 + \sqrt{\frac{\mu_2 \hat{\epsilon}_1}{\mu_1 \hat{\epsilon}_2} - \left(\frac{\hat{\epsilon}_1}{\hat{\epsilon}_2}\right)^2 \sin^2 \theta_1}} \quad (\text{A48})$$

Finally, substituting this result into Equation A46, one has a relationship for the transmission amplitude coefficient for vertical polarization:

$$\frac{E_{T0}}{E_{I0}} = \frac{2 \cos \theta_1}{\sqrt{\frac{\mu_1 \hat{\epsilon}_2}{\mu_2 \hat{\epsilon}_1} \cos \theta_1} + \sqrt{1 - \frac{\mu_1 \hat{\epsilon}_1}{\mu_2 \hat{\epsilon}_2} \sin^2 \theta_1}} \quad (\text{A49})$$

Brewster's Angle and the Critical Angle

For lossless materials, there are conditions for which reflectance is zero. The condition is trivial for horizontal polarization problems. Setting the numerator of Equation A41 to zero and assuming nonmagnetic properties, one has:

$$\cos \theta_1 = \sqrt{\frac{\epsilon_2}{\epsilon_1} - \sin^2 \theta_1}$$

Squaring both sides of the equation and using one of the fundamental trigonometric identities, one has:

$$\frac{\epsilon_2}{\epsilon_1} = \frac{n_2^2}{n_1^2} = 1$$

In other words, the two materials are identical; the interface does not exist.

For vertical polarization, setting the numerator of Equation A48 to zero and applying the same assumptions and substitutions, one gets:

$$\cos^2 \theta_1 = \frac{\epsilon_1 \epsilon_2 - \epsilon_1^2}{\epsilon_2^2 - \epsilon_1^2}$$

Inverting the equation and substituting the trigonometric identity involving \sec^2 and \tan^2 , one finally gets:

$$\tan \theta_1 = \sqrt{\frac{\epsilon_2}{\epsilon_1}} = \frac{n_2}{n_1} \quad (\text{A50})$$

The angle given by this equation is called the Brewster angle and represents the incidence angle at which no vertically polarized energy can be reflected. As an aside, since electromagnetic waves can be viewed as a linear combination of horizontally and vertically polarized components, Brewster angle reflection can be a tool for producing linearly polarized energy.

If one then substitutes Snell's law into Equation A50, one finds that at the Brewster angle,

$$\cos \theta_B = \sin \theta_2$$

which can only be true if

$$\theta_2 = \frac{\pi}{2} - \theta_B$$

Therefore, at the Brewster angle, the angle of incidence and the angle of refraction are complementary.

There are also conditions for which reflectance is total. The incident angle for which those conditions are met is called the critical angle. One can find the critical angle either by setting the reflection amplitude formulae (Equations A41 and A48) to unity or by setting the refraction angle in Snell's law to 90 deg. In either case, the critical angle is found from:

$$\sin \theta_C = \frac{n_2}{n_1} \quad (\text{A51})$$

Appendix B

Reflection and Refraction from a Thin Slab

The following figures and formulae have been lifted directly from a popular electromagnetics textbook (Reitz et al. 1979). The derivations are extensive, and interested readers are encouraged to read the source. This appendix serves only as documentation for the equations used to perform the multilayered wave propagation simulations reported in earlier sections.

Phase Shifts and Amplitude Attenuation

Two figures are required to visualize the problem of thin slab reflection and refraction. The first is useful in understanding how to account for the phase differences in energy that emanates from a plane interface because of multiple reflections and refractions of waves inside of a finite thickness layer of material. The situation is this: A plane wave traveling through a material defined by an index of refraction, N_1 , impinges upon a slab of material, N_2 , whose thickness is d . One can think of two parallel rays in the direction of the wave propagation vector in N_1 , one of which strikes the slab at O and the other which strikes at X. The incidence angle is θ_1 . The ray at O partially reflects and partially refracts into N_2 . The amplitudes of the reflected and refracted waves are determined by the formulae developed in Appendix A. The refracted portion of the incident wave travels through material N_2 where it reflects off and refracts into material N_3 . Again, this behavior is controlled by the formulae in Appendix A. The reflected portion passes back through N_2 and partially reflects back into the slab and partially refracts into material N_1 . The wave that comes out of N_2 has not only been attenuated by the material within the slab, but it has experienced a shift in phase relative to the incident ray that impinged upon the slab at X. The reduction in amplitude and the shift in phase can both be accounted for by an exponential term, $e^{i\beta}$, where:

$$\beta = 2d \frac{\omega}{c} (p + iq) \quad (B1)$$

The real part of β gives the phase shift, while the imaginary part gives the two-way attenuation of the wave amplitude within the slab. In terms of the incident angle, the dielectric constant of N_1 and the complex dielectric constant of the slab, the components of β are found from:

$$p = \sqrt{\frac{1}{2} \left[(K_{2r} - K_1 \sin^2 \theta_1) + \sqrt{(K_{2r} - K_1 \sin^2 \theta_1)^2 + K_{2i}^2} \right]} \quad (\text{B2})$$

$$q = \sqrt{\frac{1}{2} \left[-(K_{2r} - K_1 \sin^2 \theta_1) + \sqrt{(K_{2r} - K_1 \sin^2 \theta_1)^2 + K_{2i}^2} \right]} \quad (\text{B3})$$

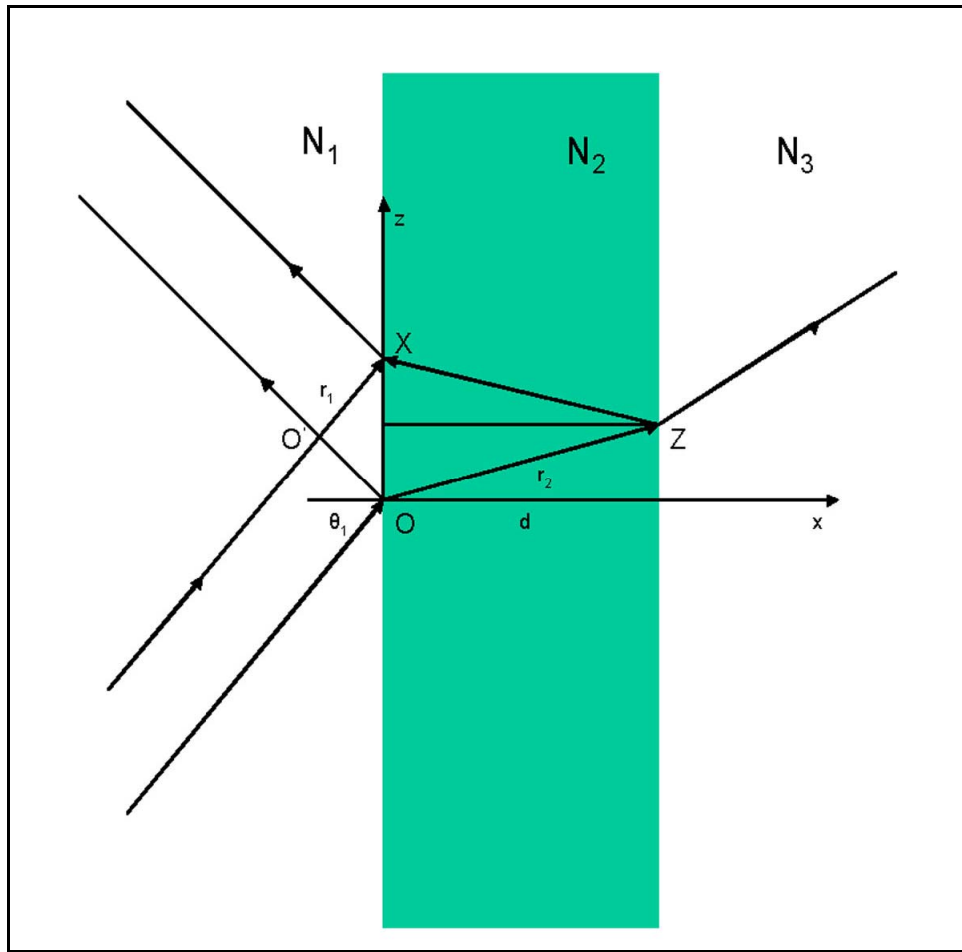


Figure B1. Paths of two rays incident on a slab of finite thickness

These equations are the same as those that relate the components of a complex dielectric constant to the components of a complex index of refraction, except that K_{2r} is replaced by $(K_2 - K_1 \sin^2 \theta_1)$. In other words, p and q are generalized versions of the real and imaginary parts of the complex index of refraction that depend on the angle of incidence.

Multiple Reflections

A second figure is useful to visualize the geometry of multiple reflections within the slab that will lead to the final formulation for reflection and transmission amplitude coefficients.

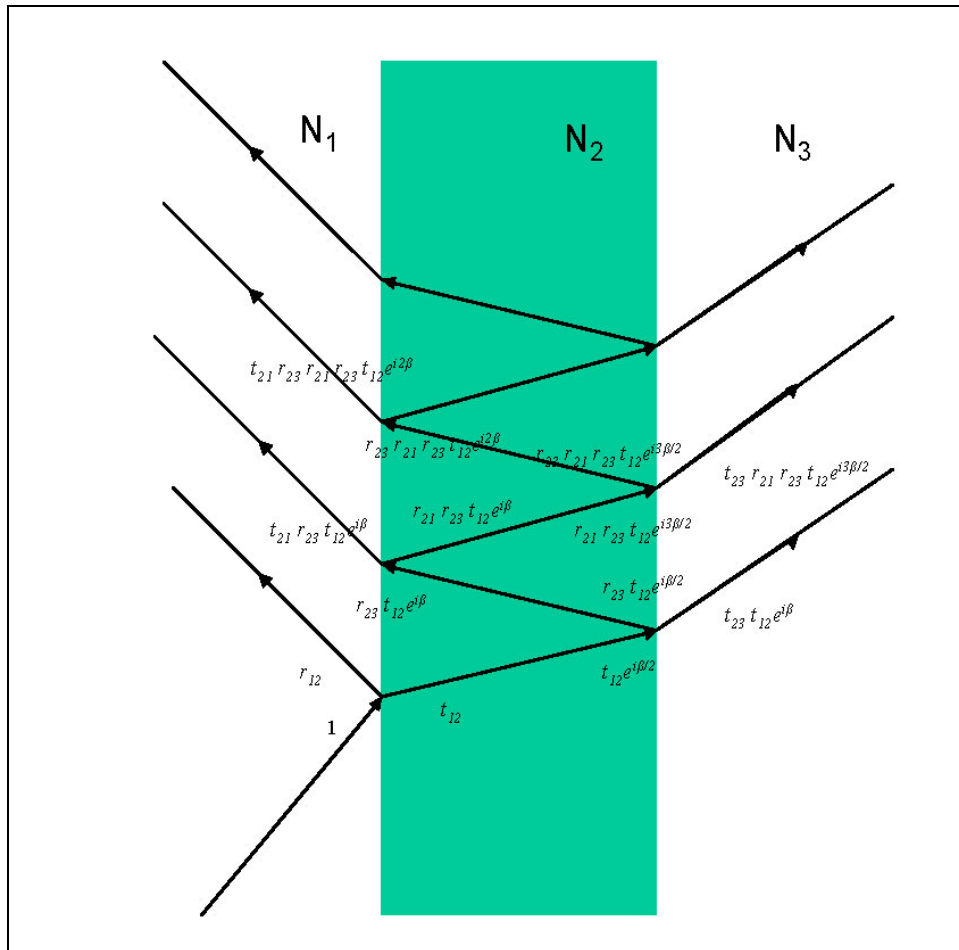


Figure B2. Reflection and refraction of a single ray incident on a slab of finite thickness

Making use of the notation that r_{ij} is the amplitude reflection coefficient for a wave traveling from material i to material j (either Equation A41 or Equation A48), and t_{ij} is the amplitude transmission, or refraction coefficient for a wave traveling from material i to material j (either Equation A42 or Equation A49), one can write down an algebraic series that adds up all of the contributions to the net amplitude reflection coefficient, r .

$$\begin{aligned}
 r &= r_{12} + t_{12}r_{23}t_{21}e^{i\beta} + t_{12}r_{23}r_{21}r_{23}t_{21}e^{i2\beta} + \dots \\
 &= r_{12} + t_{12}r_{23}t_{21}e^{i\beta} \left[1 + r_{21}r_{23}e^{i\beta} + (r_{21}r_{23}e^{i\beta})^2 + \dots \right]
 \end{aligned} \tag{B4}$$

Using the infinite series identity:

$$1 + z + z^2 + \dots = \frac{1}{1 - z},$$

one can rewrite Equation B4 as:

$$\begin{aligned}
 r &= r_{12} + \frac{t_{12}t_{21}r_{23}e^{i\beta}}{1 - r_{21}r_{23}e^{i\beta}} \\
 &= \frac{r_{12} + r_{23}(t_{12}t_{21} - r_{12}r_{21})e^{i\beta}}{1 - r_{21}r_{23}e^{i\beta}}
 \end{aligned} \tag{B5}$$

Finally, making use of the identities:

$$r_{12} = -r_{21} \tag{B6}$$

and

$$r_{12}^2 + t_{12}t_{21} = 1, \tag{B7}$$

one obtains the final form of the amplitude reflection coefficient as

$$r = \frac{r_{12} + r_{23}e^{i\beta}}{1 + r_{12}r_{23}e^{i\beta}} \tag{B8}$$

The same procedure could be used to find expressions for the amplitude transmission coefficient into material 2, the amplitude reflection coefficient for the interface between material 2 and material 3, and the amplitude transmission coefficient into material 3. However, the only coefficient needed for this study is that given by Equation B8.

It should be noted that these relationships apply for either horizontal or vertical polarization. The two-material reflection coefficients in Equation B8 come from the expressions derived in Appendix A (either Equation A41 or Equation A48), and the phase factor, β , comes from Equations B1 through B3.

REPORT DOCUMENTATION PAGE

Form Approved
OMB No. 0704-0188

Public reporting burden for this collection of information is estimated to average 1 hour per response, including the time for reviewing instructions, searching existing data sources, gathering and maintaining the data needed, and completing and reviewing this collection of information. Send comments regarding this burden estimate or any other aspect of this collection of information, including suggestions for reducing this burden to Department of Defense, Washington Headquarters Services, Directorate for Information Operations and Reports (0704-0188), 1215 Jefferson Davis Highway, Suite 1204, Arlington, VA 22202-4302. Respondents should be aware that notwithstanding any other provision of law, no person shall be subject to any penalty for failing to comply with a collection of information if it does not display a currently valid OMB control number. **PLEASE DO NOT RETURN YOUR FORM TO THE ABOVE ADDRESS.**

1. REPORT DATE (DD-MM-YYYY) February 2005		2. REPORT TYPE Final report		3. DATES COVERED (From - To)	
4. TITLE AND SUBTITLE A Computational Tool for Simulating Plane Wave Reflectance from Layered Lossy Media				5a. CONTRACT NUMBER	
				5b. GRANT NUMBER	
				5c. PROGRAM ELEMENT NUMBER	
6. AUTHOR(S) John O. Curtis				5d. PROJECT NUMBER	
				5e. TASK NUMBER	
				5f. WORK UNIT NUMBER	
7. PERFORMING ORGANIZATION NAME(S) AND ADDRESS(ES) U.S. Army Engineer Research and Development Center Environmental Laboratory 3909 Halls Ferry Road Vicksburg, MS 39180-6199				8. PERFORMING ORGANIZATION REPORT NUMBER ERDC/EL TR-05-3	
9. SPONSORING / MONITORING AGENCY NAME(S) AND ADDRESS(ES) U.S. Army Corps of Engineers Washington, DC 20314-1000				10. SPONSOR/MONITOR'S ACRONYM(S)	
				11. SPONSOR/MONITOR'S REPORT NUMBER(S)	
12. DISTRIBUTION / AVAILABILITY STATEMENT Approved for public release; distribution is unlimited.					
13. SUPPLEMENTARY NOTES					
14. ABSTRACT A computational tool was developed to visualize radar reflection coefficients for a lossy, two-layered half-space soil geometry as a function of incidence angle. Allowable input parameters include radar frequency, top soil layer thickness, and the complex dielectric properties of both soil layers. The tool is a Microsoft Excel program that can operate on any Windows-based personal computer.					
15. SUBJECT TERMS Complex dielectric properties Radar Excel Reflection coefficient					
16. SECURITY CLASSIFICATION OF:			17. LIMITATION OF ABSTRACT	18. NUMBER OF PAGES	19a. NAME OF RESPONSIBLE PERSON
a. REPORT	b. ABSTRACT	c. THIS PAGE			19b. TELEPHONE NUMBER (include area code)
UNCLASSIFIED	UNCLASSIFIED	UNCLASSIFIED		70	

